PULSATILE PROTEIN RELEASE FROM A THERMORESPONSIVE HYDROGEL: EFFECT OF DEVICE ARCHITECTURE, NANOPARTICLE AND POLYMER CONCENTRATION USING FACTORIAL ANALYSES

by

SHRUTI K GANDHI

Presented to the Faculty of the Graduate School of

The University of Texas at Arlington in Partial Fulfillment

of the Requirements

for the Degree of

MASTER OF SCIENCE IN MATERIALS SCIENCE AND ENGINEERING

THE UNIVERSITY OF TEXAS AT ARLINGTON

August 2011

ACKNOWLEDGEMENTS

I thank my advisor, Dr. Pranesh B. Aswath, for his guidance and support throughout my program. I have benefited tremendously from his counsel and disciplined approach towards problem solving. My deepest gratitude to him for his invaluable inputs which gave me direction when I needed it most.

I thank Dr. Panayiotis S. Shiakolas for providing me with his expertise in a field I am not too familiar with, for his guidance and encouragement. Whenever faced with a design limitation, his “out-of-the-box” ideas have been saviors for this research.

I cannot thank Dr. Kytai Ngyuen enough for being so generous with lending me her lab facilities and materials. Working in a drug delivery lab is a daunting task for someone without a background in the field, and I am grateful to her for trusting me and training me to work in her lab. Without her co-operation, this research would never have been possible.

I would also like to thank Dr. Yaowu Hao, for being a part of my thesis committee. His teaching style and in depth knowledge has had a great impact on me.

A special note of thanks to Aniket Wadajkar for his time and guidance. He helped me take my research from words on paper to actual meaningful data. Through the course of my research, time and again I have bothered him for several reasons and he has always been happy to help. My deepest regards for him.

I wish to express my thanks to Senai Andai, for taking time off to machine the device pieces for me-and for doing such an impressive job each time! My best wishes to him. I would also like to thank all my research group members for always being ready to help.

Juggling a job along with thesis and course work is never an easy task, and I would have never been able to do it without the support of my boss, Elaine Weiler. I thank her for being so flexible with my work schedule and just being the wonderful person that she is!

I have been very fortunate and made some wonderful friends during my stay at UTA, and I would like to thank them for being what I can most certainly call my “second family”. Aditi, Aniruddha, Anjana, Kashyap, Kirthi, Kunal, Manju, Moni, Naznine, Pam, Raksha, Rohan, Saumitra, Shreya, Sonam, and Spoorthi- you guys are the best!

Last but not the least; I would like to thank my family for all of their love and support: My parents, Jyoti and Kantilal Gandhi, for believing in my education, their constant encouragement and motivation to help me realize my goals, being a source of strength and their unconditional love. My sister and brother-in-law, Shikha and Tarun Rokadiya, for their vital guidance, support, love and inspiration. I am grateful to Govind for his unconditional support. Without his patience, sacrifices, guidance and perseverance, I would not have come this far. My family brings out the best in me and I love them very much!

May 11, 2011

ABSTRACT

PULSATILE PROTEIN RELEASE FROM A THERMORESPONSIVE HYDROGEL: EFFECT OF DEVICE ARCHITECTURE, NANOPARTICLE AND POLYMER CONCENTRATION USING FACTORIAL ANALYSES

Shruti K. Gandhi, M.S

The University of Texas at Arlington, 2011

Supervising Professor: Pranesh B. Aswath

A pulsatile thermo-responsive drug delivery device for wound healing applications was developed in this study and its drug release during 24 hours of thermal cycling was characterized. The device consisted of a temperature sensitive hydrogel of poly (*N*-isopropyl acrylamide-*co*-acrylamide) (PNIPAM-AAm) nanoparticles (LCST: 39-40°C) embedded in a poly (ethylene glycol) diacrylate (PEGDA) matrix inside a device made of poly (methyl methacrylate). The device had four different orifice geometries all with the same surface area of opening (5 mm^2): slit, cross, circle and four-circle. Bovine serum albumin (BSA) was loaded onto the hydrogel as the model protein. The effect of the orifice geometry on protein release was studied during temperature cycling alternating between 23.1 °C and 41°C. A factorial analysis was performed to study the effect of PNIPAM-AAm concentration (2% and 4% w/v), PEGDA concentration (10% and 15% w/v), and device geometry (slit and cross) on the BSA release rate during different cycles of the pulsatile release as well as the cumulative BSA released. Results indicate that

device geometry plays a significant role in regulating protein release rates with cumulative release percentages varying from 46.98% (circle) to 84.34% (slit) over 24 hours of pulsatile release. Release profiles were observed to have an initial release phase with higher release followed by a steady state release period for which the release rates for each thermal cycle were similar. The PNIPAM-AAm enhanced the protein release whereas the PEGDA limited it. These results have given us insight on the effect of device geometry, nanoparticle as well as polymer concentration of a composite hydrogel, on drug release profile from a potential thermoresponsive wound healing dressing for controlled drug delivery.

TABLE OF CONTENTS

LIST OF ILLUSTRATIONS

Figure Page

LIST OF TABLES

CHAPTER 1

INTRODUCTION

Every year, there are about 4000 deaths due to burn wounds alone in the United States and over 500,000 people requiring medical aid due to burn injuries [1], not including burn injury statistics for the armed forces. Skin wounds also result from trauma injuries and diseases such as diabetes [2]. Timely and proper medical treatment for skin wounds is of utmost importance to avoid the infections, unpleasant scars and in extreme cases, death.

Although significant attention has been given towards developing effective wound healing dressings, up until the 1960s, the research conducted did not typically result in better clinical benefits for the patient. Research made great advances when it was shown that epithelial repair rate in the skin of pigs and subsequently humans was twice as fast as compared to air-exposed wounds when polymer film dressings were used[3-5]. The first commercially available wound dressings based on these studies came out in the 1970s in the United States. A better understanding of the physiology of wound repair and subsequent advances in biotechnology have greatly increased the scope of research in this field. The roles of various growth factors in aiding wound repair at its various stages are now understood and it is now possible to manipulate the wound healing process by externally administering these factors via the wound dressing. The Vascular Endothelial Growth Factor (VEGF), one of the many signal proteins secreted during the process of wound repair has been shown to stimulate epithelialization and collagen deposition in a wound [6]. Heparin administration at wound site results in faster revascularization reduced bleeding and swelling [7].Subsequently, wound dressings have come a long way and there are a variety of dressings available these days. A broad classification can be made amongst them based on their material of construction as well as application.

Table 1.1 [8] listed below summarizes the different kinds of wound healing dressings in use.

Table 1.1 Types of wound healing dressings.

Dressing Type	**Characteristics**
Low adherent dressings	Suitable for flat, shallow wounds with low exudates
Semi permeable membranes	Promote moist environment; adhere to healthy skin but not to wound
Hydrocolloids	absorbent; conformable; may be left in place for several days
Hydrogels	Supply moisture to wounds; May be left in place several days; Need secondary dressing
Alginates	For all wound types with high exudates; highly absorbent
Foam dressings	Give degree of cushioning; may be left in place for two to three days
Antimicrobial dressings	Suitable for fungating malignant wounds; used alone or as an adjunct to other dressings

Various materials and mechanisms are utilized in the various dressing types listed in Table 1.1. While some permit loading of a desired protein/drug for specific wound site delivery, others serve the purpose of offering cushioning to the wound and absorbing exudate. However, many limitations exist for the wound dressings in use today. Most common dressings in use deliver therapeutic agents at a continuous rate. This is not in conformance with the way many vital functions in the body are regulated. Physiological processes are regulated by the transient release of biomolecules at a specific time and site [9]. A continuous drug release can lead to side effects and also require greater quantities of drugs. A controlled ON/OFF release of therapeutic agents from the wound dressing would prove to be a more efficient alternative. Using “second skin” is a standard method in use for wound healing, and it involves the use of split-thickness skin autograft [10]. However, there are many problems faced with the production of confluent epithelial sheets to treat patients. There is a time delay before cells are available for application

to the skin wound, sometimes taking weeks. Even then, hypertrophic scarring occurs in many cases [11]. Many times, the wound created at the site from where the graft is harvested also requires quick and appropriate healing. To overcome the shortcomings of the existing methods in use, a wound dressing capable of ON/OFF drug release (delivering not only antimicrobial agents, but also therapeutic agents such as growth factors), as well as imbibing desired characteristics of existing dressings is required. For this purpose, in the research work presented here, a thermo-responsive hydrogel based drug eluting device has been designed and its controlled protein release characteristics are studied.

1.1 Drive for Research

A lot of research has been carried out in the field of hydrogels with many materials having been characterized thoroughly for end applications as drug delivery mediums. Hydrogels are hydrophilic, three dimensional polymeric networks which are capable of absorbing fluids, rendering them a very versatile material in pharmaceutical formulations. [12]. In particular, classes of hydrogels have been fabricated that are sensitive to external stimuli such as pH, temperature and change in ionic concentration [13-16]. Upon application or change in an external stimulus, these hydrogels undergo a phase transition from being hydrophilic with a linear chain structure to being hydrophobic with a coiled chain structure, thus expelling the loaded drug/protein from the hydrogel. One of the most widely reported temperature sensitive hydrogels are synthesized from poly (*N*-isopropylacrylamide) (PNIPAM) and its copolymers.[17,18] [19] One such temperature sensitive hydrogel fabricated and characterized by Sabnis et al is a system of temperature sensitive ploy(*N*-isopropylacrylamide-co-acrylamide) (PNIPAM-AAm) nanoparticles embedded in a ploy(ethylene glycol) diacrylate (PEGDA) matrix.[20]. The synthesis method used to make these hydrogels, photo-crosslinking, has been widely researched since it enables hydrogels to be formed at a specific site [2, 21]. PEG-based polymers have been a material of choice as a crosslinker due to their biocompatibility and low immunogenicity [22-25]. PEGDA lead to formation of non-biodegradable hydrogels. Embedding the PEGDA crosslinked network with PNIPAM-AAm lends the hydrogel a thermo-responsive behavior. PNIPAM-AAm undergoes a phase change from a hydrophilic to hydrophobic material at 39-40°C, which can be modulated by adjusting the ratio of hydrophilic groups such as acryl

amide in the polymer [26]. Thus, it was decided to use the temperature controlled protein release behavior of this hydrogel in an end application as a wound healing device, with ON and OFF drug release behavior.

1.2 Objective of Research

The main objectives of this research are:

1. To fabricate a temperature sensitive drug eluting device using the temperature sensitive composite hydrogel system of PNIPAM-AAm nanoparticles embedded in a PEGDA matrix. Ideally, an OFF release when the hydrogel is below its phase transition temperature and an ON release when it is above.
2. In a drug eluting device, the geometry of the orifice also plays an important role in controlling the release, since not only are the hydrogel properties controlling release, but also the geometry properties, such as dimensions, surface tension, effective surface area of orifice, positioning on the hydrogel, to name a few. Also, in the pulsatile protein release desired in this study, the combined effects of the device geometry and hydrogel properties regulate the ON/OFF drug release behavior. Thus it was found vital to characterize and compare the pulsatile protein release from various geometries of the drug eluting device.
3. A full factorial study using Design of Experiments to observe the effect of several parameters on the protein release from the device.

1.3 Outline of Thesis

This section provides the basic structure of the thesis presented so as to give a reader a better understanding of the work carried out.

CHAPTER 1: Introduction

This chapter provides a brief orientation regarding the purpose of the research as well as creates a foundation for the reader to better understand the subsequent chapters presented in the thesis.

CHAPTER 2: Background

This chapter gives the reader in depth information on the progress made in the field of wound healing, hydrogels and their properties, synthesis methods and applications as drug delivery devices. This chapter specifically talks in depth about pulsatile drug release studies, temperature sensitive hydrogels and especially the hydrogel being used in this research- PNIPAM-AAm in a PEGDA matrix. A brief revision of the role of geometry on drug release profiles is also made in this section. A general idea of the approach and principle used to make the thermo-responsive drug eluting devices is also discussed here.

CHAPTER 3: Effect of Device Architecture on Protein Release

This chapter presents the various methods used and results obtained to show the effect of four different device geometries on the pulsatile protein release; the four different geometries all had the same effective surface area, but different shapes. Thus, while some had smaller dimensions, others were spaced over the length of hydrogel. The geometries studied here were a slit, cross, circle and four-circles.

CHAPTER 4: Factorial Analysis

This chapter provides a full factorial analysis using a design of experiments (DOE) software from Stat-Ease (Stat-Ease, Minneapolis, MN), to illustrate the effect of multiple factors on the protein release from two different device architectures. DOE is the statistical analysis of the effect of certain input parameters and the interactions between them, on the output of a process. It identifies the relationship between the input factors and the response of a system and also helps in giving a predicted response for conditions that have not been studied experimentally. It reduces the number of runs required to predict process behavior. A full factorial design was used to provide insight on the effect of device geometry, nanoparticle and polymer concentrations on the protein release rates from the device at various stages of pulsatile release. It helped identify the interactions between the parameters and how they control the release behavior.

CHAPTER 5: Summary and Future Work

This chapter summarizes the results obtained in this study and provides suggestions for future work to further develop this research.

CHAPTER 2

BACKGROUND

2.1 The Science of Wound Healing

To develop a treatment method for healing of wounds, it is important to understand the mechanism behind it as well as the role of various mediators and growth factors. A wound can be defined as any disruption of the integrity of the skin, mucous membrane, organ or tissue. This process can be divided into three overlapping phases of inflammation, proliferation and modeling [27]. Figure 2.1 below illustrates the different phases of wound healing.

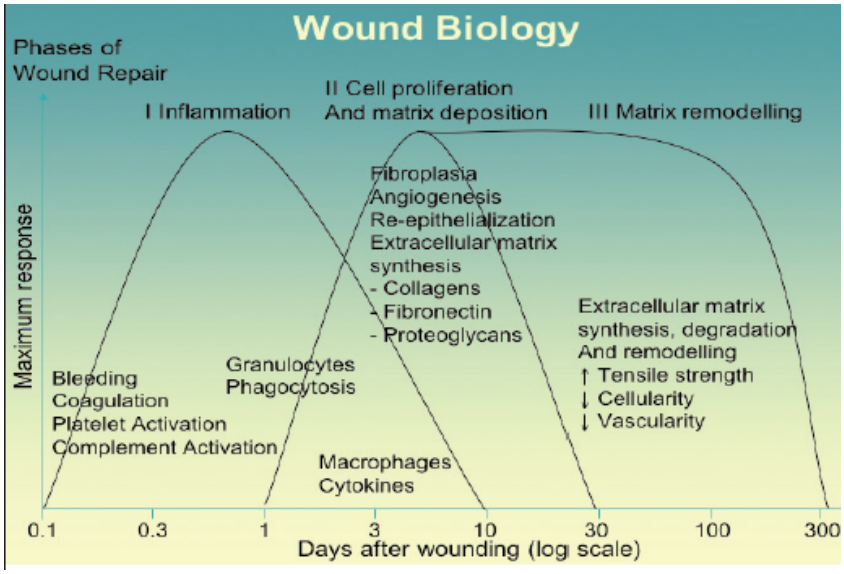

Figure 2.1 Phases of wound healing and respective mediators and processes associated with it [27].

The inflammation phase is generally complete within the first 48 to 72 hours and is characterized by bleeding, coagulation, platelet cell activation and activation of the complement cascade. The proliferation stage phase starts around the 3rd day and is characterized by three important changes to the injured tissue: epithelialization, angiogenesis and provisional matrix formation, which ultimately lead to the formation of granulation tissue. Growth factors such as the vascular endothelial growth factor (VEG

secreted by keratinocytes plays an important role in the formation of the granulation tissue and collagen deposition [6]. The last phase of maturation and remodeling can last from one to up to one year. In this phase, the type III collagen is replaced by the mature type I collagen and apoptosis occurs to reduce the number of fibroblasts, keratinocytes and macrophages, leading to a healed wound with a minimal scar and return to near normal tissue architecture and function [28]. If proper care is not taken during wound repair, it may lead to a chronic wound or keloid scar.

2.2 Wound Dressings

There are several different kinds of wound dressings available, especially since the development of new materials over the past few years. A general requirement of a wound healing dressing is given below [8]:

1. Capable of maintaining a high humidity at the wound site while removing excess exudate.
2. Free of particles and toxic wound contaminants.
3. Non-toxic and non-allergenic.
4. Capable of protecting the wound from further trauma.
5. Can be removed without causing trauma to the wound.
6. Impermeable to bacteria.
7. Thermally insulating.
8. Will allow gaseous exchange.
9. Comfortable and conformable.
10. Require only infrequent changes.
11. Cost effective.
12. Long shelf life.

A general classification of wound dressings based on materials is given below [29]:

1. Transparent films- Usually consist of polyurethane films coated with and adhesive. These films are elastic and conformable, act as a bacterial barrier and have high moisture-vapor permeability.

2. Hydrocolloids- Often composed of materials such as carboxymethylcellulose, polyisobutylene, pectin and gelatin. They consist of an adhesive wafer laminated to either a film or foam layer.
3. Hydrogels- composed of hydrophilic polymers which immobilize large quantities of water to form a semi-solid gel. These dressings can be applied and removed with minimal pain, and provide a conducive environment for wound healing.
4. Alginates- are derived from seaweed and these fiber dressings are used for the treatment of exuding wounds. These fibers absorb exudate and form a gelatinous mass which entraps fluid and debris. Removal of such dressings is possible in a non-traumatic fashion since calcium alginate is readily dissolved in saline solution.
5. Surgical wound repair- Split thickness autograft is the most common method of surgical wound repair; however, it does not always lead to ideal wound healing and sometime leads to the formation of overgrowth of epithelial tissue over deep embedded granulation tissue leading to scar formation.[11]
6. Skin replacement and substitutes- Green et al [30] have conducted pioneering work in developing confluent sheets of epithelial cells to treat wounds. However, there are several problems associated with healing wounds via this route, mainly, the time required to develop the epithelial sheets. Several interactive dressings also exist, e.g. *BIOBRANE™ (Dow B. Hickman Inc., Sugar Land, TX, USA)* which consists of an open knit nylon filament coated with collagen and backed with a silicone rubber membrane to prevent dehydration of the wound site. Biobrane serves as a temporary, synthetic skin.

2.3 Hydrogels for Drug Delivery Applications

Since the drug eluting device developed in this study is based on a temperature sensitive composite hydrogel, this section provides an overview of hydrogels for drug delivery. Hydrogels are three-dimensional, hydrophilic, polymeric networks capable of imbibing large amounts of water or biological

fluids. Chemical and physical cross-links between these networks provide them with structural integrity and make them insoluble [31].

Hydrogels have found vast applications in biomedicine because their high water content and soft texture give them a very close resemblance to natural living tissue and as well as make them biocompatible.[32][12]. Thus, hydrogels have been developed to be used as contact lenses, implants, drug delivery devices and membranes to name a few [33]. In the field of drug delivery, hydrogels are especially advantageous because they provide protection to drugs, peptides, proteins from any potential harsh environment at the drug delivery site [34].

2.3.1 Environmentally Responsive Hydrogels

The swelling behavior of certain hydrogels is dependent on their environment. This class of hydrogels is said to be stimuli sensitive or environmentally responsive. Such hydrogels may be responsive to environmental stimuli such as pH, electric charge, magnetic field and temperature [35]. In general, Figure 2.2[35] illustrates how swelling behavior changes typically with the application of external stimuli and leads to drug delivery.

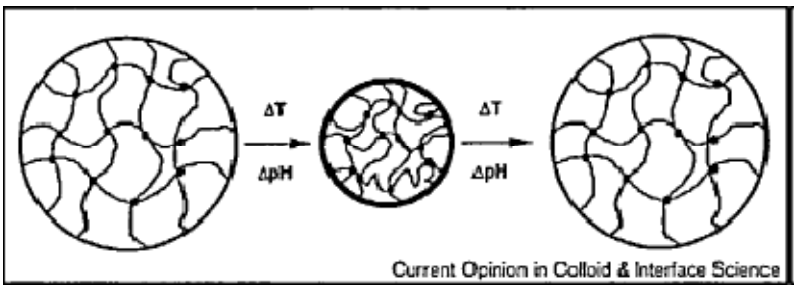

Figure 2.2 Swollen hydrogels exhibit abrupt change, e.g. expanded (left) to collapsed (center) and back to expanded state (right) with change in external stimuli such as pH or temperature. This process is generally reversible and influences the molecular distance between consecutive cross-links, allowing a drug or protein to be released via molecular diffusion [35].

1. *pH Sensitive Hydrogels*

pH sensitive hydrogels contain pendant acidic or basic groups that either accept or donate protons in response to the environmental pH. Swelling of a hydrogel increases as the external pH increases in case

of weakly acidic (anionic) groups, but decreases if the polymer contains weakly basic (cationic) groups [36]. The most common anionic pH sensitive polymers are based on poly (acrylic acid) (PAA) and its derivatives [37].

2. *Magnetic-sensitive Hydrogels*

It involves encapsulating magnetic nanoparticles with preformed natural or synthetic polymers which have loaded drugs/protein on them. Magnetic fields can be used to direct and trigger the release from these particles at specific sites. [38].

3. *Electric-sensitive hydrogels*

Electrically responsive systems consist of polyelectrolytes, thus they are also sensitive to pH. These hydrogels can either bend or swell under the effect of an electric field. Chitosan gels have been studied as matrices for electrically controlled drug delivery [39].

4. *Temperature Sensitive Hydrogels*

These are probably the most researched class of stimuli-sensitive hydrogels. These hydrogels are able to swell or deswell as a result of change in local temperature in the surrounding fluid. The composite hydrogel used for pulsatile drug delivery in this research is a thermo-sensitive composite hydrogel consisting of PNIPAM-AAm embedded in a PEGDA matrix. PNIPAAM and its copolymers have been widely characterized for controlled drug delivery purposes. [19, 35] A more detailed discussion on temperature sensitive hydrogels is given in the next section.

2.3.2 Temperature Sensitive Hydrogels

Temperature sensitive hydrogels can be classified into negatively thermo-sensitive and positively thermo-sensitive reversible hydrogels [12].

Negative thermo-sensitive hydrogels have a lower critical solution temperature (LCST), below which the hydrogel is in its hydrophilic, swollen state. In this state, the hydrogen bonding between the polymer and water molecules is responsible for polymer swelling. Above the LCST, hydrophobic interactions become dominant, thus the hydrogel shrinks and releases all the water along with any loaded drug/protein on it. Poly (*N*-isopropyl acrylamide) (PNIPAM) is used as a common negative thermo-

sensitive hydrogel with and LCST of 32℃. The LCST of these polymers can be modulated by incorporating hydrophilic or hydrophobic groups in their structure. By adding acrylamide monomers to PNIPAM structure, the LCST can be raised up to 45 °C [26]. Negative thermo-sensitive hydrogels have a significant application in controlled drug delivery. They can be utilized for on-off drug release, thus leading to a more efficient drug release system [40-42].

A positive thermo-sensitive hydrogel has an upper critical solution temperature (UCST). Thus, upon cooling, the hydrogel shrinks and deswells. Above the UCST, the hydrogel is in a swollen state. Polymers with UCST of near physiological temperatures (~37℃) exist as free flowing liquids at ambient temperatures, but gel at body temperature. This property has been exploited by Cappello et al [43] who developed novel protein polymers “ProLastins”, which when injected in the body, form a firm stable gel within minutes.

A US patent [44] describes a drug delivery device for the transdermal drug delivery of bioactive molecules at a therapeutically effective rate. The system consists of a thermo-responsive gel for controlled release of the bioactive molecules.

2.4 PNIPAM based hydrogels

Due to LCSTs near physiological temperatures, PNIPAM and its copolymers are a popular choice for developing drug delivery systems. Some of the systems using this polymer are discussed here in this section.

Varghese et al [45] developed a thermoresponsive hydrogel based on PNIPAM/chondroitin sulfate via precipitation polymerization. Precipitation polymerization leads to porous hydrogels, thereby increasing the drug diffusion and release rate. Chondroitin was added to increase the thermal response of the hydrogel. The hydrogels exhibited stable thermal behavior, following a volume change of 75% while cycling the temperature between 20 and 45 ℃.

Comb type grafted poly (*N*-isopropyl acrylamide-co-acrylic acid) hydrogels have been developed which are dual temperature and pH sensitive. Due to dual response, rapid release from these hydrogels has been shown to be effective. [46]

Coughlan et al [47] investigated the effect of drug physicochemical properties on swelling/deswelling kinetics and pulsatile drug release from thermoresponsive PNIPAM hydrogels. They used hydrogels of PNIPAM copolymerized with hydrophilic monomers and hydrophobic monomers (alkyl methacrylate) and used *N*, *N*′-methylenebisacrylamide (MBA) as the cross linker. The effect of hydrophilic and hydrophobic drugs on hydrogel swelling behavior was studied and pulsatile release experiments were carried out. Hydrophobic drugs decreased the swelling rate whereas hydrophilic drugs increased it. A pulsatile on-off release was also achieved.

2.5 Pulsatile Drug Release

Pulsatile drug release is defined as the rapid and transient release of a certain amount of drug molecules within a short period of time immediately after a pre-determined off-release period. [42]. A pulsatile drug release is preferred over continuous release for several reasons. Most vital processes in the body follow a rhythmic pattern requiring only optimal amounts of therapeutic agents. This optimal level is attainable by periodically fluctuating drug concentration. Moreover, administering large amounts of drugs/biomolecules can cause undesired side effects. [48]. Figure 2.39, 9] below illustrates the difference between a pulsed and conventional continuous release.

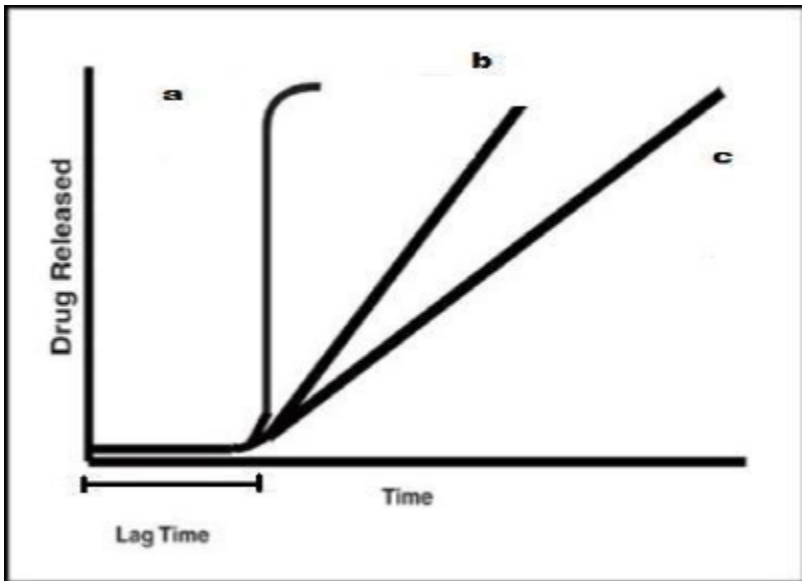

Figure 2.3 Common release profiles: (a) Pulsatile release (b) and (c) continuous and extended release [9].

Temperature-sensitive hydrogels can be utilized for pulsatile release and PNIPAM and its copolymers have been known to show a controlled pulsatile release behavior by oscillating the temperature above and below the LCST.

Brazel et al [49] investigated the pulsatile local delivery of thrombolytic and antithrombotic agents using poly (*N*-isopropyl acrylamide-co-methacrylic acid) hydrogels. Streptokinase and heparin were loaded onto these hydrogels and their release characteristics were observed under pulsatile conditions. While it was possible to pulse the streptokinase release, the much smaller heparin molecule showed little difference in release between the collapsed and swollen state.

The work of Lue et al [50] involved developing thermally on-off switching membranes of PNIPAM immobilized in track etched polycarbonate films. The cross linked PNIPAM network was immobilized into micro-porous track etched polycarbonate films. The effective pore sizes were regulated by the degree of swelling and shrinking of the hydrogel around its LCST. Figure 2.4[50] below explains the on-off mechanism for this system.

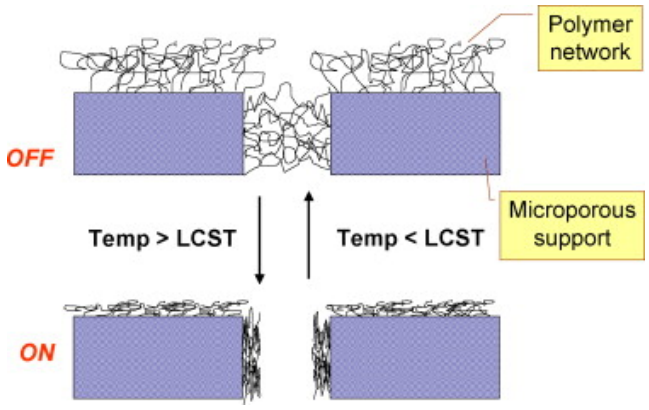

Figure 2.4 Schematic of on-off valve mechanism of PNIPAM polymer grafted onto PC membranes. These membranes exhibited fast and reversible swelling changes in the 30-40°C range. As can be understood, the number of pores in the membrane as well as the pore size will affect the release behavior. Thus, the geometry of the opening becomes an important parameter in determining the release rates [50].

Dinarvand et al [51] investigated the effect the device opening would have, to a certain extent in their research of using thermo-responsive hydrogels for on-off release of molecules. They developed a thermo-responsive valve based delivery device, the schematic of which is shown in Figure 2.5[51]. At temperatures above the LCST, the hydrogel deswells, leading to a reduction in volume of hydrogel and increase in the free volume within the valve (valve in open state). Upon reducing the temperature, the hydrogel reswells, obstructing release (valve in closed state).

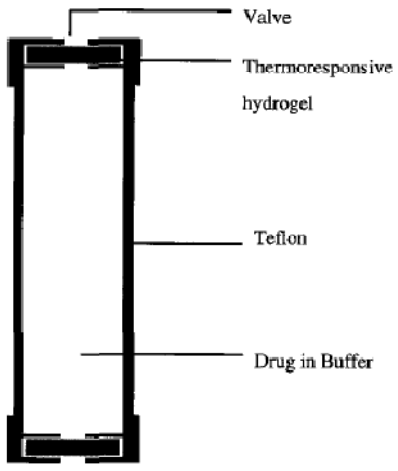

Figure 2.5 Schematic diagram of a thermoresponsive valve-based delivery device [51].

A similar approach has been adopted as the principle controlling drug release in the drug eluting dressings for wound healing for this research. In the study carried out by Dinarvand, the release studies were carried out for devices with 1 and 2 apertures per valve, and a difference in the drug release was noticed.

A study on the effect of thermal cycling on the properties of PNIPAM hydrogels revealed that repeated thermal cycling leads to the formation of cracks on the surface of the hydrogel and a decreased degree of swelling at temperatures below LCST. [52]. Thus, any drug delivery system made using these hydrogels have a limitation on their life span depending on the number of times thermal cycling is done.

2.6 PNIPAM-AAm/PEGDA Composite Hydrogels

The work described in previous sections consisted of thermo-responsive hydrogels made from bulk. The hydrogel discussed here essentially consists of PNIPAM-AAm nanoparticles embedded in a PEGDA matrix made via photo-polymerization. Photo-polymerization of hydrogels is a beneficial method to synthesize hydrogels since these hydrogels can be formed at a specific site [19]. PEG based photo cross linking is particularly advantageous for biomedical applications because of their biocompatibility and ease of use. PEG incorporated with diacrylate group forms non-biodegradable hydrogels. [24, 53]

Sabnis et al [20] formulated a photo-crosslinked PNIPAM-AAm/PEGDA thermoresponsive hydrogel, the methods of which have been used to in this current research as well. Figure 2.6[20] below is a schematic explaining the principle of photo-polymerizable thermo-responsive composite nanoparticle hydrogels.

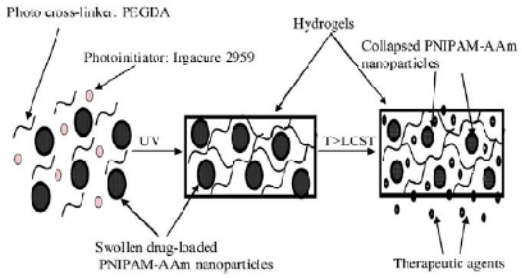

Figure 2.6 Principle of drug release from photo-crosslinked thermoresponsive composite nanoparticle hydrogels [20].

In comparison with bulk hydrogels, the drug loading approach adopted here is more beneficial. In bulk hydrogels, drugs are loaded in the bulk gel by allowing the hydrogel to swell in a drug solution or by mixing it with the monomers, initiators, solvents, etc [54]. Such methods may cause harm to the loaded drug/proteins by solvent reactions and excessive heating. In this method, drugs are mixed with nanoparticle suspension at room temperature.

The effects temperature, PEGDA concentration, PNIPAM-AAm concentration and PEG molecular weight on the protein release profiles of these hydrogels using a factorial analysis was investigated. PEG molecular weight was found to have the most significant effect on swelling behavior, with low molecular weight polymers inhibiting the swelling. Low swelling means less water diffusion and thus lower drug release. A higher temperature and PNIPAM-AAm concentration obviously enhanced the drug release, whereas the PEGDA concentration inhibited it.

The results from the work carried out by Sabnis lays the groundwork for the current research presented in subsequent chapters. Since the release experiments are continuous here, pulsatile release of these hydrogels was carried out from a specially fabricated device, and the profiles were characterized and their dependence on the device geometry, PNIPAM-AAm concentration and PEGDA concentration studied using a full factorial study.

CHAPTER 3

EFFECT OF DEVICE ARCHITECTURE ON PULSED PROTEIN DELIVERY FROM A THERMO-RESPONSIVE HYDROGEL

3.1 Introduction

Hydrogels sensitive to external environmental stimuli have been a topic of interest for many years and significant progress has been made towards development of drug delivery systems responsive to external stimuli such as temperature, pH and electric field [16]. Amongst the thermo-responsive hydrogels, PNIPAM and its co-polymers has been widely researched for applications in drug delivery and tissue engineering since its phase transition temperature is in the range of physiological temperatures [13, 19, 20, 55].

The hydrogel system in use for experiments here comprises of PNIPAM-AAm nanoparticles embedded in a PEGDA polymer matrix. Continuous protein release experiments and their dependence on factors such as nanoparticle concentration, polymer concentration and temperature were studied by Sabnis et al [20]. However, for drug delivery applications, a pulsatile release is preferred over a continuous dosage of drug. In the body under physiological conditions, many processes are regulated by the transient release of biological substances at a specific time and site. A pulsatile drug release can be defined as the rapid and transient release of a certain amount of molecules within a short period immediately after predetermined off-release periods. There are several advantages of a pulsed drug delivery, such as reduced dose frequency, easier drug targeting, and reduced side effects. [9].

A drug delivery device responsive to change in temperature was developed and the results of its pulsed protein release behavior and dependence on device architecture is presented in this chapter. An attempt was made to create a system with an ON/OFF release which is regulated by the temperature. In

the PNIPAM-AAm/PEGDA hydrogel system used here, the thermo-responsiveness of this hydrogel comes from the PNIPAM-AAm nanoparticles, which at an LCST of 39 °C – 40 °C, undergo a phase change from a hydrophilic, linear chain structure (hydrogen bond interactions are strong) to a hydrophobic , coiled structure, thus shrinking and pushing the water out along with any loaded protein/drug. The PEGDA acts a cross-linker that serves as a matrix to hold all the nanoparticles. The model protein used in these studies was Bovine Serum Albumin, because it is very similar in molecular weight to other therapeutic agents.

Figure 3.1 below depicts the underlying principle used to apply the hydrogel properties towards controlling the drug release.

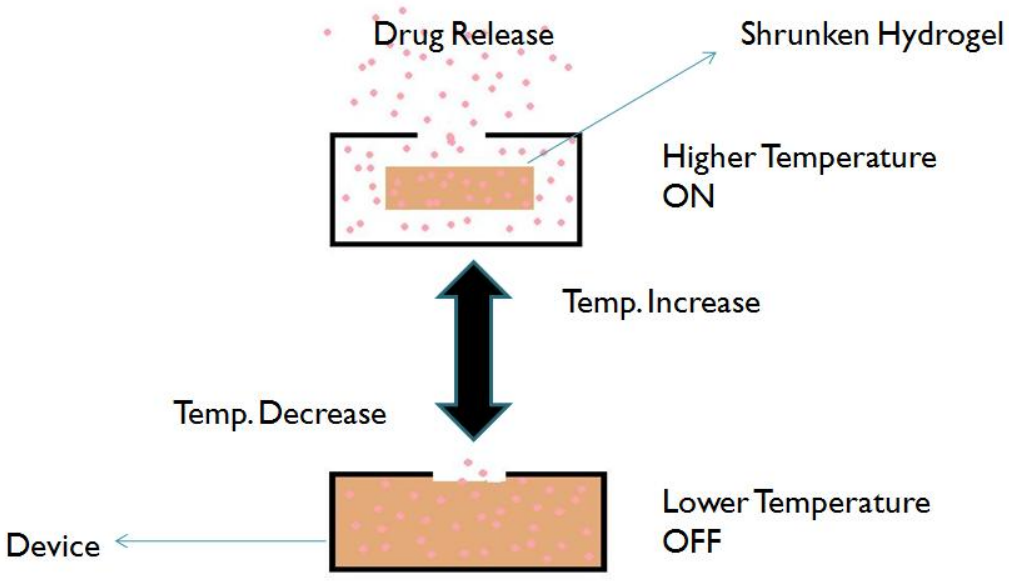

Figure 3.1 Principle of ON-OFF drug release control mechanism from device.

When the hydrogel is incorporated with a device with an opening, below the LCST, the hydrogel is swollen and this swollen state acts as a seal for the drug release from the device. The drug release here is solely regulated by the diffusion rate of the loaded drug through the hydrogel and out through the device opening. Once the temperature is increased beyond the LCST, the hydrogel shrinks and there is

an increase in the free volume inside the device for the drug to be released along with the water and out through the device opening. [56]

3.2 Materials

If not specified, all chemicals were purchased from Sigma-Aldrich (St. Louis, Missouri). Poly (ethylene glycol), anhydrous dichloromethane, triethylamine, acryloyl chloride, potassium carbonate (K_2CO_3), magnesium sulfate ($MgSO_4$), ethyl ether, N-isopropylacrylamide, N,N′-methylenebisacrylamide, potassium persulfate, and sodium dodecyl sulfate, poly(methyl methacrylate) sheets, styrene butadiene O-rings (Grainger Inc.), clear plastic hinged boxes (Durphy Packaging Co.), aluminum slab, silicone oil, plumbers putty.

3.3 Methods

The methods described below to prepare the PNIPAM-AAm nanoparticles; PEGDA polymer and composite hydrogel are based on the methods used by A. Sabnis et al. [20]

3.3.1 Preparation of poly(N-isopropylacrylamide-co-acrylamide) nanoparticles

PNIPAM-AAm nanoparticles (220.6 ± 7.7 nm diameter) with a lower critical solution temperature of 39℃ - 40℃ where prepared using the following m ethod. Aqueous solution (100 ml) containing N-isopropylacrylamide (1.3644 g), acrylamide (0.1756 g), N, N'-methylenebisacrylamide (0.262 g) and sodium dodecyl sulfate (0.0439 g) was stirred under argon gas for 30 minutes. Potassium persulfate (0.624 g) was added, and radical polymerization was carried out at 70 ℃ for four hours under an atmosphere of argon. The resulting solution was cooled to room temperature and dialyzed with a (6-8 kDa) molecular weight cut–off against deionized water for four days to remove the unreacted monomers and surfactants. The deionized water was replaced with fresh stock 3 times a day. The resulting solution was then lyophilized to obtain nanoparticles. The lower critical solution temperature (LCST) of these nanoparticles was measured using a lab assembled optical set up calculated at 50% transmittance. The

nanoparticle size was determined using a Dynamic Light Scattering machine. A suspension of the PNIPAM-AAm nanoparticles was prepared and beamed with a laser. The laser scatters the particles and takes measurements of the nanoparticle size and dispersion.

3.3.2 Preparation of poly(ethylene glycol) diacrylate

Poly (ethylene glycol) diacrylate (PEGDA) was synthesized with an average molecular weight of 3.4 kDa and 8 kDa respectively. The following protocol was used: 12 g of PEG (3.4 kDa/8 kDa) were dissolved in 36 ml of anhydrous dichloromethane. 1.3 ml of triethylamine was added to the solution which was then bubbled with argon gas for five minutes. 0.61 ml acryloyl chloride was dissolved in 10 ml of dichloromethane which was then added drop wise to the above solution over a period of 2 hours. The above solution was then stirred under argon gas for 2 days on an ice bath. The reaction mixture was then washed with 2 M potassium carbonate to separate the dichloromethane phase, followed by drying with anhydrous magnesium sulfate. The PEGDA polymer was then precipitated in ethyl ether and filtered and dried for 12 hours under vacuum at room temperature (20 ℃ - 25 ℃).

3.3.3 Preparation of photo-polymerized thermo-responsive hydrogels

A stock solution of PNIPAM-AAm in deionized water was prepared. The model protein, Bovine Serum Albumin, was added to this stock suspension at a concentration of 5 % (w/v) and incubated at 4 ℃ for 4 days and subsequently dialyzed (10,000 MWCO) against DI water for 3 hours. A sample of this DI water was taken and stored for subsequent protein characterization to calculate the loading efficiency of the protein onto the nanoparticles. Then, 800 µL of the BSA loaded nanoparticle suspension was taken and 0.15 g of PEGDA was dissolved in it. 200 µL of the IRGACURE 2959 photo-initiator solution (0.015 g/ml) was then added to the above BSA loaded solution to make a 1 ml total solution with PEGDA concentration of 15 % (w/v), and PNIPAM-AAm concentration of 4 % (w/v). To make the hydrogel, 100 µL of this solution was poured into the device cavity and exposed to ultraviolet light at about 10 mW/cm^2 for roughly 5 minutes. Three samples (n=3) were prepared for each different device geometry. There have been previous studies done by Sabnis et al [57], where the optimal concentration of photo-initiator to be used and duration of UV exposure have been investigated.

3.3.4 Experimental Setup

Due to the requirement of pulsing the temperatures of the hydrogel, from room temperature (23.1 ℃) to above the LCST (41℃), a special set up was desi gned to assist the device and the hydrogel loaded in the device to reach the LCST in the shortest span of time possible. For this, an aluminum slab 8” x 6” x 5” with a centrally placed cylindrical cavity 5” in diameter and 4” in depth was placed inside a low temperature furnace maintained at 41 ℃. Silicone o il was poured into this cavity. A rotor, rotating at 10 rpm with the help of low voltage motor, with plates to hold the devices was mounted onto this slab and suspended in the silicone oil. This entire set up was allowed to heat up to 41℃ for about 24 hours to ensure the system had reached steady state. It was then used to carry out protein release experiments at 41℃. Figures 3.2 A and 3.2 B, respectively, show t he set up discussed here. Room temperature protein release was carried out by placing the hydrogel loaded devices on an orbital shaker, at room temperature (23.1℃).

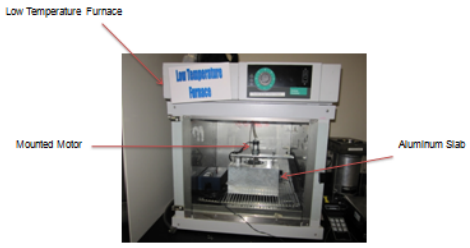

(a)

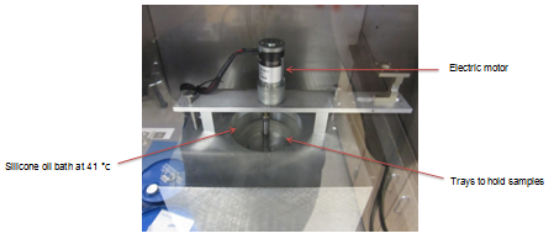

(b)

Figure 3.2 Experimental setup for (a) protein release studies above the LCST at 41°C and (b) a close up view of the setup used for testing at 41 °C.

In order to know the heating and cooling profile of the hydrogel in the device, a wired thermocouple was placed in the hydrogel to monitor the temperature at its core and the temperature profile through one heating and cooling cycle was noted and plotted against time.

3.3.5 Fabrication of drug eluting device

Drug eluting devices were fabricated using poly (methyl methacrylate) (PMMA). This material was chosen as it is easy to machine, relatively inert, biocompatible, can be used in temperatures ranges required of this study, and has a low specific heat (1.46 kJ/kg K).

PMMA sheets were machined to form a base plate 2.5 cm x 2.5 cm with a circular cavity of diameter 1.7 cm and 1 mm in depth. A butadiene rubber O-ring with inner diameter of 1.27 cm and actual width of 0.238 cm was fitted into the cavity, making the effective cavity diameter roughly 1.27 cm and approximate volume to be 0.126 cc.

Slide in covers of PMMA with four different opening geometries were fabricated. All openings had the same effective surface area of 5 mm^2. The four different geometries used were a slit, centrally located cross, centrally located circle and four equally spaced circles. Figure 3.3 displays the four different opening geometries used as covers for the protein eluting device. These four geometries were chosen so as to give a good variation in the geometries. While, the slit and cross geometries have a more polygonal geometry, the circle and four circle geometries are circular. Even though all the geometries are centrally located on the hydrogel, the slit and four-circle geometry provide better access the hydrogel (edges as well as center).

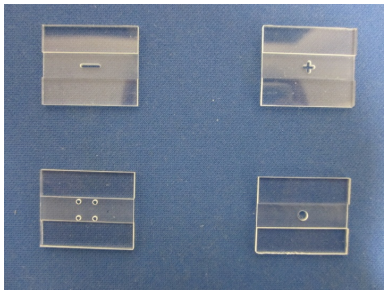

Figure 3.3 The four geometries of the openings in the drug delivery device, all of which had the same opening area of 5 mm^2.

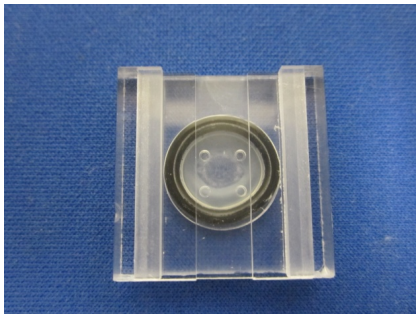

Figure 3.4 Drug delivery device with 4 holes with the O-ring in place. The hydrogel with the protein loaded in it is placed in the chamber within the O-ring.

These devices were placed in a clear plastic hinged box 2.54 cm x 2.54 cm and inside height of 8 mm (Durphy Packaging Co.) and 1 ml of DI water was added to the box, such that it just wets the opening on the cover plate. When immersed in the silicone oil bath at 41℃, the box was sealed with plumber's putty.

3.3.6 Effect of device architecture on protein release

To evaluate the effect of the various device architectures on the protein release, the device containing the protein loaded nanoparticle hydrogels (n=3) were pulsed from room temperature (23.1℃) to the LCST (41℃) and alternated back and forth at specified time intervals over a period of 24 hours. The time duration at room temperature and LCST was 2 hours (OFF) and 1 hour (ON), respectively. At these predetermined time points (2, 3, 5, 6, 8, 9, 11, 12, 14, 15, 17, 18, 20, 21, 23, 24 hours), the DI water from the boxes were replaced with fresh DI water. The samples thus collected at the time points were analyzed using the BCA (Bicinchionic Acid) protein assay (Pierce, Rockford, IL), following the manufacturer's instructions, to characterize the amount of protein released from the hydrogel. Runs were also taken to observe continuous release at the same predetermined time points at both 23.1 ℃ and 41℃.

The data procured from the BCA assay was used to calculate the following:

Loading Efficiency

$$Loading\ Efficiency\ (\%) = \frac{Original\ Protein\ Amount - Protein\ Amount\ in\ Dialysis\ Solution}{Original\ Protein\ Amount} \times 100$$

Protein Release Rate (mg/hour)

$$Protein\ Release\ Rate = \frac{Amount\ of\ released\ protein}{Time\ in\ which\ above\ protein\ amount\ is\ released}$$

The protein release rate was plotted against time to represent the variation in the protein release rate between the ON and OFF cycles of the temperature pulsing.

Protein Release (%)

$$Protein\ Realease\ (\%) = \frac{Amount\ of\ released\ protein}{Amount\ of\ loaded\ protein} \times 100$$

The cumulative protein release was calculated and plotted as the % of initial loading against time to represent the protein release profile.

3.4 Results and Discussion

3.4.1 PNIPAM-AAm nanoparticles

The LCST of the PNIPAM-AAm nanoparticles prepared was found out to be 39℃-40℃. It was calculated by plotting the % transmittance vs. the temperature of the nanoparticles. There is a sudden drop in the transmittance when the nanoparticles reach the LCST due to a phase transition and coiling up of the polymer chains. This drop in transmittance was observed at 39℃ - 40℃ for the nanoparticles us ed in this research. Figure 3.5 shows the % transmittance vs. temperature (℃).

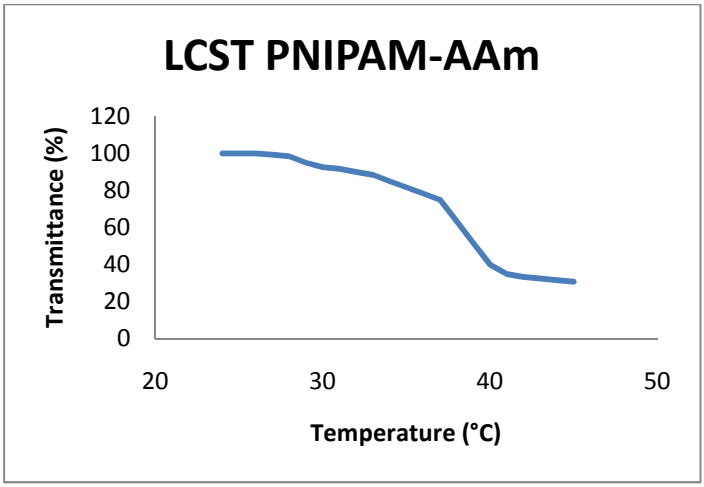

Figure 3.5 A %Transmittance vs. Temperature graph to find LCST of PNIPAM-AAm nanoparticles. The %Transmittance falls sharply at around 39-40°C, implying the nanoparticles undergo a phase change at that temperature.

The nanoparticle size was observed to be approximately 220.6 ± 7.7 nm with a polydispersity index of 0.132, suggesting that the nanoparticles are fairly mono-dispersed. Figure 3.6 below illustrates the size distribution of the nanoparticles as obtained from the Dynamic Light Scattering machine.

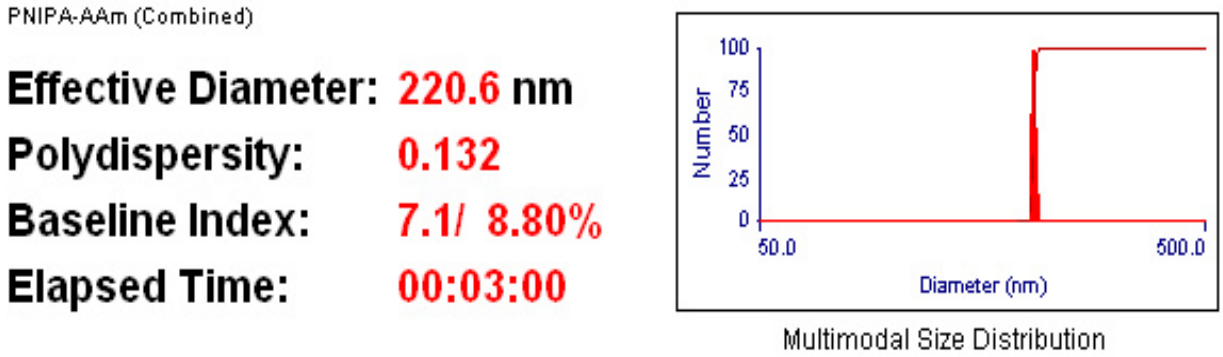

Figure 3.6: Particle size and distribution of PNIPAM-AAm nanoparticles obtained from dynamic light scattering.

3.4.2 Experimental Setup

The experimental setup was designed to achieve minimal heating and cooling times of the hydrogel loaded in the devices during drug release. Figure 3.7 illustrates the heating and cooling temperature profile of the device.

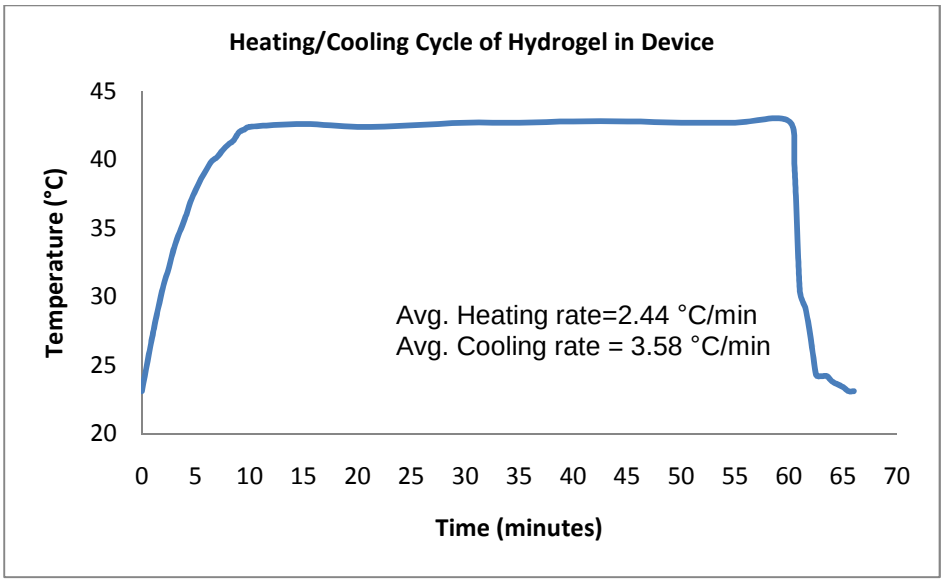

Figure 3.7 Heating/Cooling Cycle of composite hydrogel inside the device.

It was observed that the hydrogel heated up to 41℃ (above the LCST) within the first 7 minutes, followed by a steady state for rest of the heating cycle. When removed from the heating setup, it took less than a minute for the hydrogel to cool down to room temperature i.e. 23.1 ℃.

3.4.3 Effect of Device Architectures on Protein Release Rate

3.4.3.1 Continuous Release Study

A continuous protein release profile was obtained for all four different device geometries both at room temperature (23.1 ℃) and above the LCST (41 ℃) ov er a period of 24 hours. Both releases, above and below LCST started out with a fairly steady state release pattern which eventually plateaus out after approximately 8 hours. Thus, maximum protein is released within the first 8 hours of testing, after which the release becomes negligent due to small concentration gradients. Figure 3.8 shows the release profile at 23.1℃.

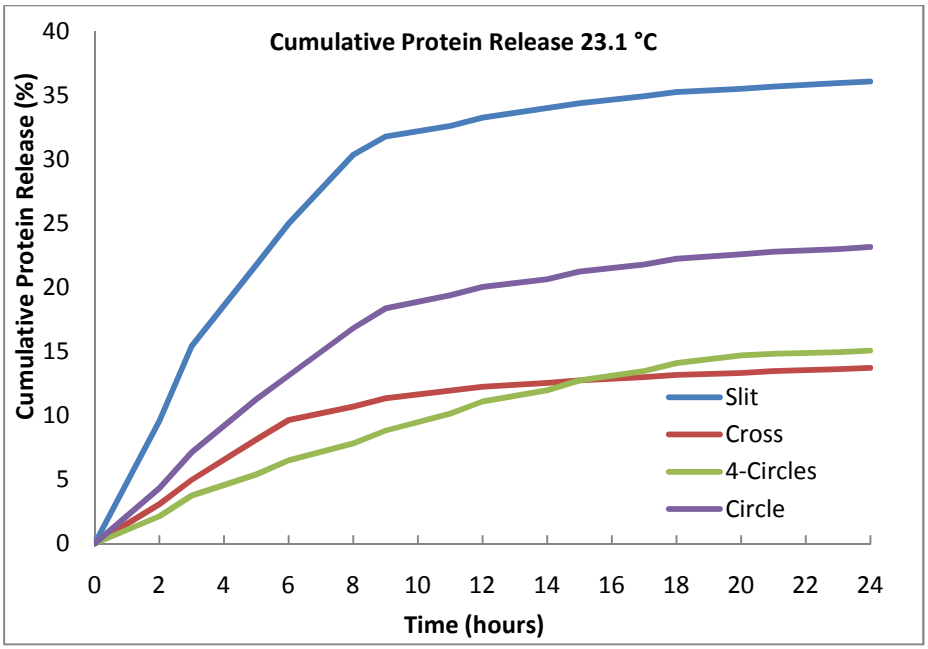

Figure 3.8 % Cumulative protein release vs. time graph for continuous release at 23.1 °C for 24 hours.

Below LCST, the protein release is only due to diffusion through the swollen hydrogel matrix. There is no phase change in the nanoparticles that release any of the protein loaded in them. A release was observed from all geometries, thus it is safe to say that the swollen hydrogel does not provide a 100% effective seal to the protein exiting through the device geometry.

A big difference was observed in the cumulative protein released from the different geometries. The maximum protein release was observed from the slit geometry (up till 35 %), followed by the circle geometry (23%). The 4- circle and cross geometries had comparable release amounts at 15% and 13%, respectively. This is a very interesting result, since all geometries have the same effective surface area. A better understanding of the release characteristics can be made once the release profile above the LCST is studied. Figure 3.9 below shows the release at 41 °C.

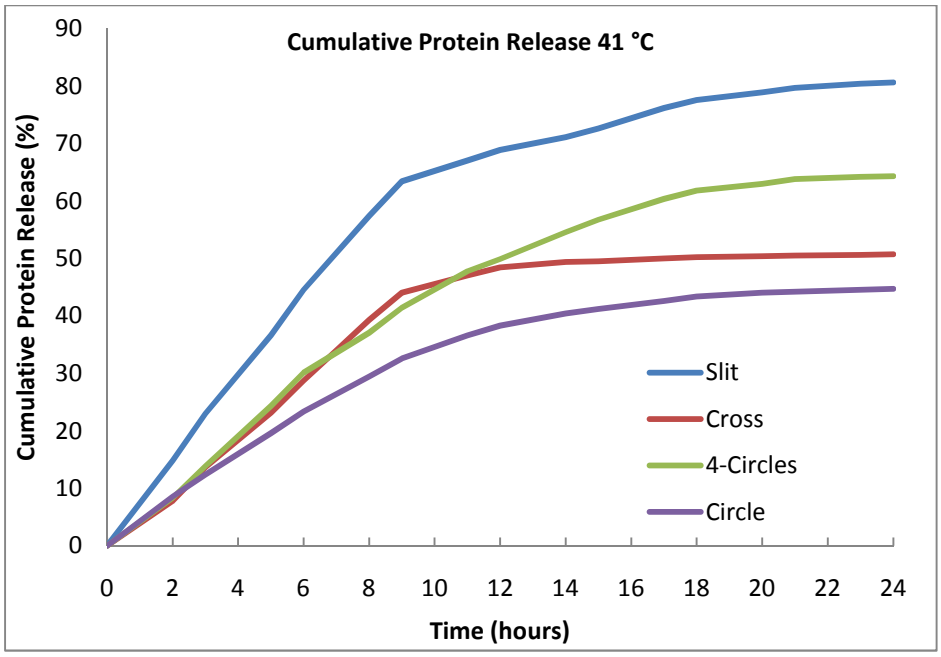

Figure 3.9 % Cumulative protein release vs. time graph for continuous release above LCST at 41 °C.

Above the LCST, the PNIPAM-AAm nanoparticles have undergone a phase change and shrunk, expelling the loaded protein out. As observed, the slit geometry has the highest release even above the LCST, with a cumulative BSA release of 80%. The 4 circle geometry and cross geometry do start out with almost an identical release pattern for the first 8 hours, however, while the cross geometry release reaches a plateau region post 8 hours with negligent release, the 4 circle geometry tends to continue release before gradually reaching a plateau region much later . The circle geometry follows the same trend as the 4 circle, but with a lower cumulative release.

In both cases, at room temperature and above LCST, the slit geometry had the highest release. This greater release is because the slit spans through the diameter of the hydrogel, allowing easier access to the hydrogel at the center as well as towards the edge of the cavity. The slit and cross geometry can be clubbed together, as can the circle and 4 circle geometries, they have similar release curves (although different release percentages).

It has been observed that when the hydrogel is photo-polymerized in the device cavity, due to surface tension, the surface forms a slight concave meniscus, thus having greater thickness towards the edges as compared to the center. This could be the reason that the slit geometry and to a certain extent, the 4-

circle geometry above the LCST have a greater release since they both provide better access to the hydrogel near the edges where it is greater in thickness, thus carrying more protein. The circle and cross geometries have a lower release above the LCST since they provide easy access only to the center of the hydrogel (which is thinner), not the edges.

During release at room temperature, release from the 4-cirlce geometry goes down drastically and is quite similar in value to the release from the circle geometry. This can be attributed to the fact that, below the LCST, the hydrogel is in a swollen state, thus occupying the entire cavity and pushing against all walls on all sides. The individual diameters of the four circles in the 4 circles in the 4 circle geometry are small enough to provide a more effective seal (due to surface tension). The diameter of each circle in the 4 circle geometry is 1.26 mm and that of the circle geometry is 2.52 mm.

To summarize the results from the continuous protein release:

1. Steady state release occurs up till approximately 8 hours for all geometries, both above and below the LCST, after which the release becomes negligent.
2. The slit and cross geometries, and the circle and 4 circle geometries have similar release curves, respectively.
3. At room temperature, highest release is by the slit geometry, followed by the circle, 4 circle and cross geometry, in that order.
4. At 41 °C, highest release is by the slit, followed by the 4 circle, cross and circle geometries, in that order.
5. A concave meniscus is formed while making the hydrogel in the device cavity, making the hydrogel thicker towards the edges and thinner towards the center.
6. Geometries that provide easier access to the edges as well as center of the hydrogel have a higher release above the LCST. (Slit and 4 circles)
7. Geometries that have effective smaller diameter/length of opening have lower release at room temperature since the swollen hydrogel provides better seal and it is harder for water to seep through due to surface tension.

3.4.3.2 Pulsatile Protein Release Study

A pulsatile protein release profile was obtained for all four geometry devices. Devices were subjected to a two hour OFF period, where they were maintained below the LCST of the PNIPAM-AAm nanoparticles at room temperature (23.1 °C) and a one hour ON period, where they were maintained above the LCST of the nanoparticles at 41 °C. Figure 3.10 illustrates the cumulative protein release profiles. A pronounced pulsed release was observed for all geometries, with a more or less plateau release during the OFF cycle and an incremental release during the ON cycle. In the 24 hours of pulsing, effective ON time was 8 hours, the remaining 16 hours being release during the OFF cycle.

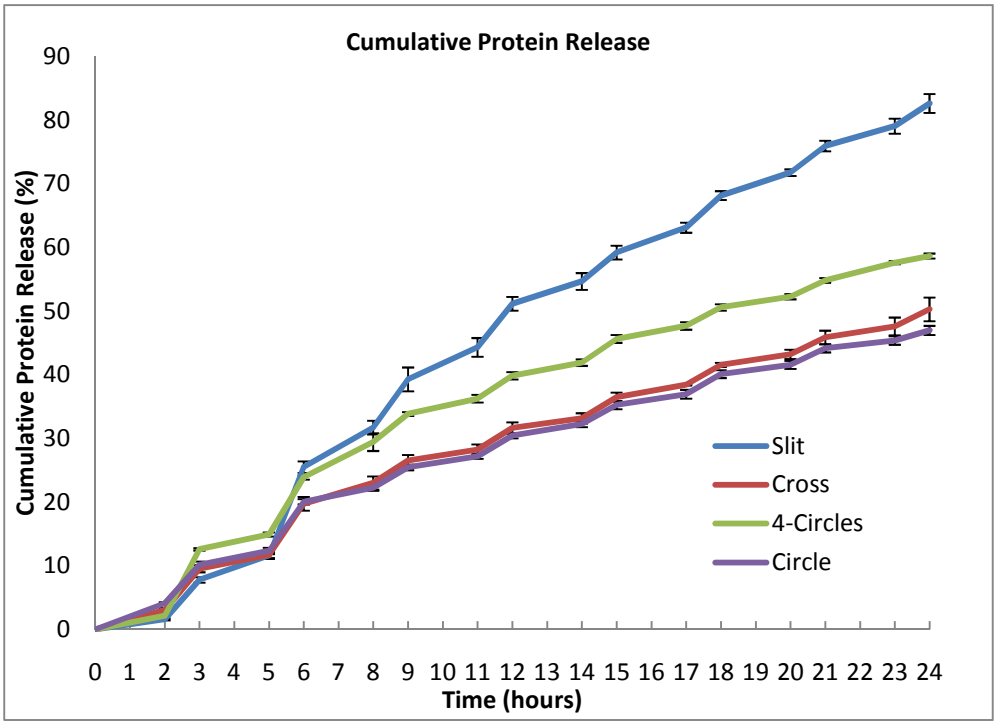

Figure 3.10 Cumulative release vs. time graph during 24 hours of thermal cycling for all four geometries.

As expected from the results of the continuous release tests, the slit geometry showed the maximum cumulative release, followed by the 4 circle geometry and then the cross and circle geometries with very similar release profiles. Again, this release pattern can be attributed to the reasoning that geometries which provide easier access to the edges as well as center of the hydrogel, release a higher cumulative amount of protein.

The protein amounts released during the first six hours of testing (or two pulse cycles) are much larger than in subsequent cycles. Thus it would be safe to divide the release profile into two main stages: initial release and steady state release:

Initial Release The initial release comprises of the first two thermal cycles (up until 6 hours). This stage comprises of the 1st OFF cycle, 1st ON cycle, 2nd OFF cycle and 2nd ON cycle. During the 1st OFF cycle, the release is minimal, with all geometries releasing more or less the same amount of protein. The release here is purely based on diffusion through the hydrogel matrix, and of course through the device geometry. The 1st and 2nd ON cycles have a significant release percentage, since there is a burst release from the hydrogel. However, due to the constraint on the protein release by the geometry, no pronounced burst release effect is observed.

Steady State Release After the first two thermal cycles, subsequent cycling above and below the LCST of the nanoparticles gives us more or less repetitive protein release amounts for each ON and OFF cycle. We do not observe a strictly OFF release below LCST, which can be explained by the reasoning that all the protein released in the ON phase may not diffuse out through the device, and instead some amount settles on the hydrogel surface when it swells again at room temperature. This protein amount easily diffuses out of the device geometry over the 2 hours of the OFF cycle.

Over a period of 24 hours of testing, the slit geometry released 82% of the original drug loaded in the hydrogel. Due to the low concentration gradients, attaining close to 100% cumulative release would span a much larger time frame. However, in the same 24 hours, the circle and cross geometries released only approximately 50% of the original protein loaded. Thus, it would be safe to say that we could observe a higher cumulative release if we increase the time duration of these tests. Thus, by modifying the geometry, we can also modify the life of the wound healing dressing that can be fabricated based on the research of this study.

A comparison of the release rates through the thermal cycles support the conclusions drawn from the percentage cumulative release graph. Figure 3.11 depicts the release rates for all four geometry devices over a period of 24 hours.

The slit and 4-circle geometries show the highest release rates in the initial release stage, since they provide better access to the edges and center of the hydrogel. In the ON release cycle during the initial release stage, release rates as high as 127 µg/hr (slit) and 98 µg/hr (4 circles) are observed, whereas the release rates drop down to a range of 20 µg/hr - 30 µg/hr during the OFF cycle.

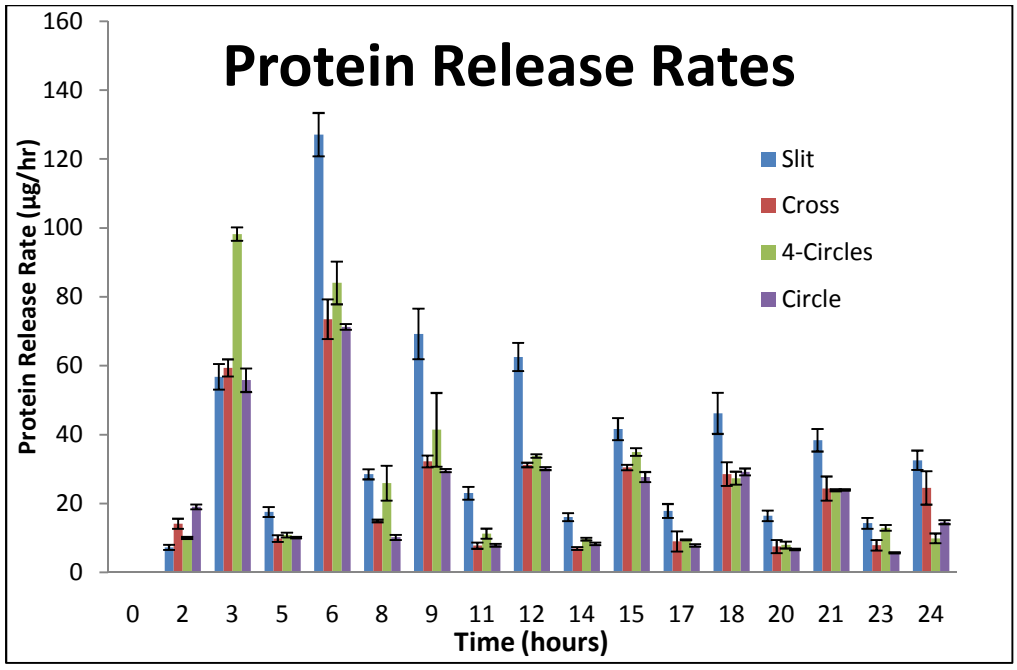

Figure 3.11 Protein release rates over 24 hours of pulsatile release for all four geometries. During the steady state stage of the release, near-constant release rates were observed for each of the device geometries, respectively, for the ON and OFF cycles.

3.5 Conclusions

The following points summarize the conclusions drawn from the results of the experiments carried out in this chapter:

1. The device architecture plays a significant role in the protein release profile from the hydrogel. Not only is it important to study the release behavior of the protein from the hydrogel, but it is also important to monitor the release through the device opening geometry.
2. An approximate ON/OFF release behavior is possible by thermal cycling of the hydrogel inside the device. Studies carried out over 24 hours had a total of 8 hours of ON time and 16 hours of OFF time.

A cumulative release as high as 82 % (slit), and as low as 46% (circle) was observed for this time period.

3. Devices which have geometry that provide easier access to both the center as well as the edge of the hydrogel in the device have a higher protein release and release rate due to the formation of the concave meniscus when the hydrogel is poured into the device and photo-polymerized. Changing the material of construction may change these properties.
4. During thermal cycling (2 hours of cooling-1 hour of heating), after an initial release stage (first six hours), the release rates steady off with a more or less constant ON and OFF release rates for all four device geometries.

CHAPTER 4

PULSATILE PROTEIN RELEASE FROM A THERMORESPONSIVE HYDROGEL BASED DEVICE: A FACTORIAL ANALYSIS

4.1. Introduction

In Chapter 3, we observed how device architecture affects protein release from a thermoresponsive hydrogel during thermal cycling. Based on those results, in this chapter, a design of experiments approach is utilized to study the effect of several other factors along with device architecture on the protein release from the PNIPAM-AAm/PEGDA hydrogels during thermal cycling.

Design of experiments (DOE) is the statistical analysis of the effect of certain input parameters and the interactions between them, on the output of a process. This approach has found wide use in almost all industries around the world. A well planned experiment can shed much light on the effect of input parameters on the response variables of a process. It has a significant advantage over the more traditional one-factor-at-a-time approach, which involves holding certain factors constant while alternating the levels of one variable. This method is inefficient and very often yields misleading results. An easier approach is to use a factorial design. They require a minimal number of runs but allow you to identify interactions in the process. An analysis done on these experiments gives useful insight on the cause-effect relationship between factors and the responses of a process. They also allow for the identification of the significant input parameters. It is also possible to optimize the response using this approach. The work of Fisher, R. A [58] has been the most influential in the field of statistical theory for the development of the design of experiments approach. Several DOE software is available these days to help the researcher analyze more complex processes and generate various response curves.

The design of experiments software, Design Expert from Stat-Ease Inc. (Minneapolis, MN), was used to illustrate the effect of individual and multiple factors on the protein release rates from the composite

hydrogel system. A full factorial study was done using three factors and their effect on the protein release rates as well as cumulative release during different stages of thermal cycling were analyzed.

4.2 Materials

If not specified, all chemicals were purchased from Sigma-Aldrich (St. Louis, Missouri). Poly (ethylene glycol), anhydrous dichloromethane, triethylamine, acryloyl chloride, potassium carbonate (K_2CO_3), magnesium sulfate ($MgSO_4$), ethyl ether, N-isopropylacrylamide, N,N′-methylenebisacrylamide, potassium persulfate, and sodium dodecyl sulfate, poly(methyl methacrylate) sheets , styrene butadiene O-rings (Grainger Inc.), clear plastic hinged boxes (Durphy Packaging Co.), aluminum slab, silicone oil, plumbers putty.

4.3 Methods

4.3.1 Preparation of poly(N-isopropylacrylamide-co-acrylamide) nanoparticles

PNIPAM-AAm nanoparticles (220.6 ± 7.7 nm diameter) with a lower critical solution temperature (LCST) of 39℃ - 40℃ were prepared using the same procedu re described in Chapter 3.

4.3.2 Preparation of poly(ethylene glycol) diacrylate

PEGDA (3.4 kDa) was prepared using the same procedures described in Chapter 3.

4.3.3 Factorial analysis using design of experiments

A full factorial study using Design Expert, a design of experiments software from Stat-Ease Inc. (Minneapolis, MN) was carried out to depict the effects of three independent variables on the protein release rate of the composite hydrogel from the device during thermal cycling. Since the number of independent variables here are three, a total of 2^3 = 8 runs were required for the design. Using *n=3* (replicates), a total of 8 x 3 = 24 runs were carried out for the full factorial analysis. The three independent variables included the PEGDA concentration (P: 10% and 15% w/v), PNIPAM-AAm concentration (N: 2% and 4% w/v) and device geometry (G: categorical factor: slit and cross). Table 4.1 lists out the low and high levels for the full factorial design.

Table 4.1 High and low levels of design factors

Level	PEGDA Concentration P (% w/v)	PNIPAM-AAm Concentration N (%w/v)	Geometry G
Low (0)	10	2	Cross
High (1)	15	4	Slit

Based on the results obtained in Chapter 3, the cross and slit geometries were chosen for this factorial study since they both had polygonal geometries, similar shape of protein release curves and while one had maximum protein release in 24 hours (slit), the protein release from the other was at the other extreme.

A midpoint analysis was carried out to further develop the model and enhance its accuracy. Approximate mid-levels were chosen for the PEGDA concentration (12.5% w/v) and nanoparticle concentration (3% w/v). A mid-level of the device geometry is not possible since it is a categorical factor. Again, the midpoint analysis had three replicates, taking the total number of runs required for the full factorial study to 30. Table 2 lists the actual values of the full factorial design and the six responses analyzed during the pulsatile release study.

Table 4.2 Full Factorial Design

	Factor 1	Factor 2	Factor 3	Response 1	Response 2	Response 3	Response 4	Response 5	Response 6
Run	**A:N**	**B:P**	**C:G**	**1st Off Cycle**	**1st On Cycle**	**2nd Off Cycle**	**2nd On Cycle**	**Steady State On Cycle**	**Cumulative Release- 24 hr**
	% w/v	% w/v		µg/hr	µg/hr	µg/hr	µg/hr	µg/hr	%
1	2	10	Slit	5.917	63.122	15.227	132.599	74.271	78.586
2	2	15	Cross	8.323	51.62	6.005	56.197	30.143	33.711
3	4	15	Slit	5.624	61.889	15.512	136.472	81.606	78.867
4	4	10	Slit	6.915	88.53	20.059	146.213	88.589	88.8
5	2	15	Cross	8.646	52.148	6.035	57.078	30.613	34.711
6	2	15	Slit	0.636	43.581	13.164	97.684	64.237	67.118
7	4	10	Cross	15.834	74.21	14.631	79.376	42.29	61.357
8	2	15	Slit	0.842	43.757	13.428	97.919	64.647	67.67
9	4	15	Cross	14.895	59.249	8.851	69.283	33.547	52.027
10	4	10	Cross	16.568	75.679	15.189	80.608	43.17	63.433
11	4	10	Slit	6.974	85.303	20.499	143.983	89.469	87.835
12	3	12.5	Slit	6.886	78.496	16.098	137.058	82.251	74.861

Table 4.2 – continued

13	4	10	Cross	16.216	74.975	14.895	79.904	43.053	62.402
14	4	15	Cross	15.071	61.948	9.966	80.08	30.261	48.323
15	4	15	Slit	5.213	60.95	15.071	135.709	80.256	77.47
16	2	10	Slit	6.181	63.004	15.71	132.188	73.33	78.494
17	3	12.5	Slit	6.71	78.554	16.744	137.528	84.657	75.989
18	3	12.5	Cross	11.492	70.633	12.93	59.953	35.131	44.388
19	2	10	Cross	10.524	71.102	7.443	66.29	39.004	43.261
20	3	12.5	Cross	11.815	71.043	13.311	60.422	36.129	45.016
21	2	15	Cross	7.913	50.623	5.536	55.2	29.439	32.314
22	2	10	Cross	11.287	67.52	7.883	66.29	38.887	43.353
23	3	12.5	Slit	6.789	78.026	16.538	137.176	83.836	75.726
24	4	15	Slit	5.125	60.716	14.749	135.415	79.552	76.681
25	3	12.5	Cross	9.966	65.997	12.783	57.136	34.838	42.215
26	4	10	Slit	7.15	87.122	20.411	143.279	89.821	87.993
27	2	10	Slit	6.123	63.708	16.186	132.89	73.801	78.783
28	4	15	Cross	12.46	56.96	10.729	71.161	32.843	50.508
29	2	15	Slit	0.871	44.872	14.631	97.156	64.647	68.294
30	2	10	Cross	10.935	66.819	7.619	66.995	39.6502	43.143

4.3.4 Preparation of photo-polymerized thermoresponsive hydrogels

PNIPAM-AAm/PEGDA composite hydrogels were prepared using the same procedure as described earlier in Chapter 3. The model protein BSA was loaded at 5% (w/v) concentration on to the PNIPAM-AAm nanoparticles. These hydrogels were photopolymerized in the previously described devices with a slit and cross geometry of opening.

4.3.5 Effect of factors on protein release

To evaluate the effect of the factors on protein release, the BSA loaded composite hydrogels in the device (*n=3*) were subject to thermal cycling, alternating temperatures from room temperature (23.1 ℃) to above the LCST (41℃) for 24 hours. Each thermal cycle comprised of 2 hours at room temperature (OFF) and one hour above the LCST at 41 ℃ (ON). The same experimental setup described earlier in Chapter 3 was used. At predetermined time points (2, 3, 5, 6, 8, 9, 11, 12, 14, 15, 17, 18, 20, 21, 23, 24 hours); 1 ml of the DI water was collected and replaced with fresh DI water. The samples collected were then analyzed for BSA content using the BCA protein assay (Pierce, Rockford, IL).

4.4 Results

In the previous chapter, we have concluded that the device geometry plays an important role in determining the protein release behavior from the thermoresponsive composite nanoparticle hydrogel. In this chapter, we have investigated how the geometry is affecting the release during different stages of pulsatile release, along with two other factors, PEGDA concentration and PNIPAM-AAm concentration, using a full factorial design. A detailed discussion of the effect of the factors on the protein release and the inferences drawn from the factorial analysis is done here.

From the results of the pulsatile protein release experiments presented in Chapter 3, two distinct phases of protein release were identified, an initial release period comprising of the first 2 thermal cycles (1^{st} OFF, 1^{st} ON, 2^{nd} OFF and 2^{nd} ON cycles) and a steady state release period comprising of the

subsequent remaining thermal cycles. Thus, the effect of the factors was studied on the protein release rate (µg/hour) for the 1st OFF, 1st ON, 2nd OFF and 2nd ON cycles of the initial release stage, as well as the 1st ON cycle of the steady state release state. The effect of the factors on the cumulative protein released during 24 hours of pulsing was also evaluated.

4.4.1 First OFF Cycle

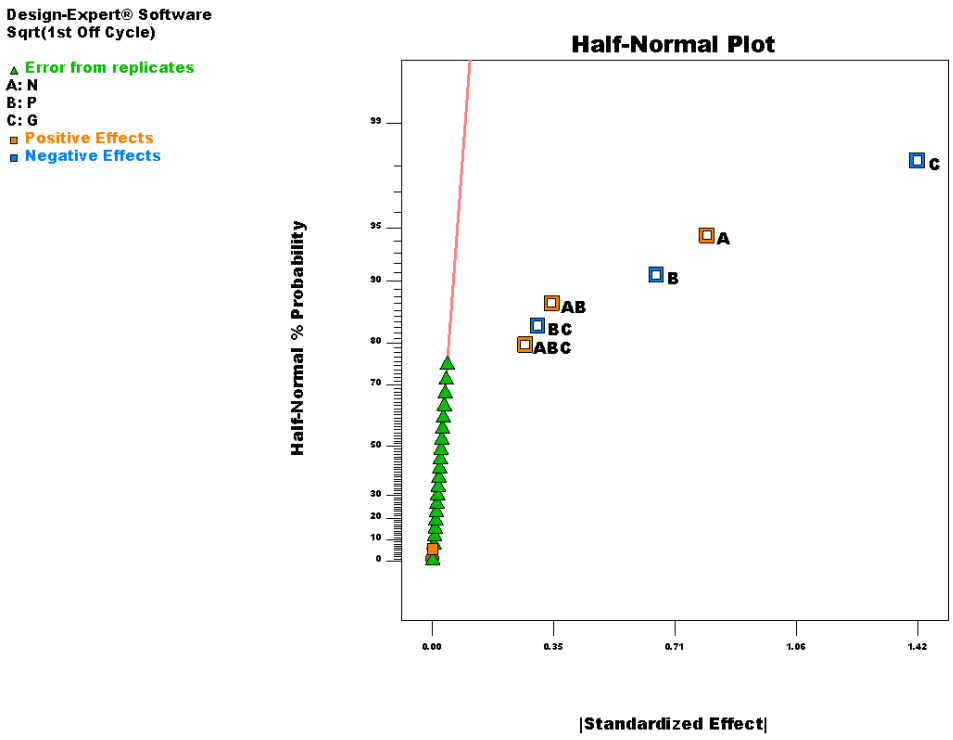

Figure 4.1 Half normal plot for 1st OFF cycle where A (N) corresponds to the PNIPAM-AAM, B (P) corresponds to PEGDA and G corresponds to the device geometry (slit or cross).

A half normal probability plot provides information on factors that are important and those that can be ignored. It also gives information on whether the factors have a positive (increased protein release) or negative (lower protein release) effect on the response. Figure 4.1 shows the half normal probability plot for the 1st OFF cycle. The absolute value of an effect and the estimates of the errors are represented by squares and triangles, respectively. The most significant effects are those to the right of the plot, where as the effects that are close to the left region are those which are insignificant and are those that occur by

chance. These are categorized as errors. The positive effects are those that bear a direct relationship with the response whereas negative effects bear an inverse relationship.

During the 1st OFF cycle, the most significant effects that control the protein release rate are geometry (positive effect), nanoparticle concentration (positive effect), PEGDA concentration (negative effect), and to a lesser extent a combination of the individual factors. To gain a better understanding of these interactions, response surface diagrams were developed for the protein release rate from the slit as well as cross geometry. Response surface diagrams are very useful in modeling curved quadratic surfaces and can pinpoint minimum and maximum response when it lies within the factor region. One of the most common RSD is a central point design where all the factor values are at the extremes and the center point is the midpoint between the numerical factors. Center points for categorical values cannot be chosen and both factors have to be chosen, doubling the number of center points.

Slit:

The equation for protein release rate from the slit geometry during the 1st OFF cycle in terms of actual factors and combined effect of factors was obtained from the factorial analysis. The predicted protein release can be calculated for any combination of factors within the range provided in Table 1 by equation below.

$$\textbf{R in the 1}^{\textbf{st}}\textbf{ OFF Cycle for Slit (µg/hr)} = [7.92301 - (1.14774)N - (0.56424)P + (0.12396)NP]^2$$

Where R is the protein release rate, P is the PEGDA concentration and N is the PNIPAM-AAm concentration and NP is the combined effect of the PNIPAM-AAm and PEGDA concentrations.

Figure 4.2 depicts the response surface diagram for the protein release during the 1st OFF cycle for the slit geometry. From the figure, it can be seen that the nanoparticle concentration and PEGDA concentration have an antagonistic effect on the protein release. The hydrogel is below the LCST during this cycle, thus the release rates have a low value range from 0-8 µg/hr. A maximum release is observed at the high level of nanoparticle concentration (4% (w/v)) and low level of polymer concentration (10% (w/v)), whereas a minimum release is observed for the exact reverse conditions. The actual midpoint

values lie above the predicted curve surface. This suggests that the model might be improved by performing additional experiments at intermediate levels of the factors.

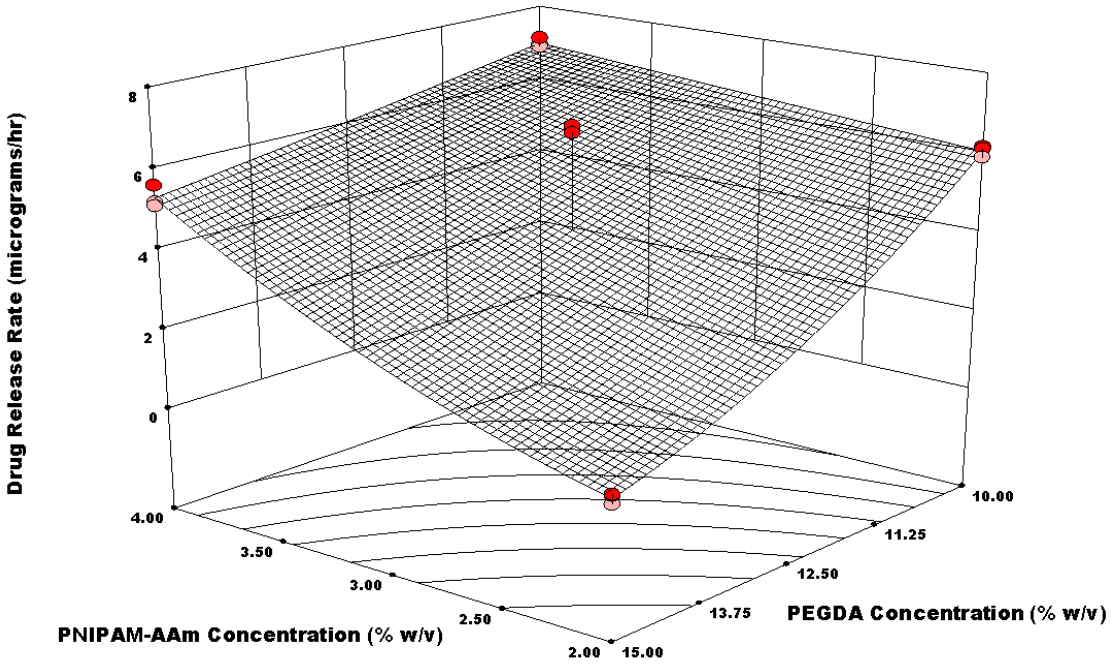

Figure 4.2 Response surface diagram for release rate from slit geometry during 1st OFF cycle.

Figure 4.3 is the contour diagram illustrating the role played by PNIPAM-AAM and PEGDA concentration on protein release rate during the 1st OFF cycle. From figure 4.3, it can be concluded that protein release rate increases with an increase in nanoparticle concentration and decrease in PEGDA concentration. The release rate is more sensitive to nanoparticle concentration beyond a value of around 3 % (w/v). During the 1st OFF cycle, the desired release rate is minimal. Thus, for example, a release rate of 2 µg/hr can be maintained over a nanoparticle concentration range of 2 – 2.75 % (w/v) and a polymer concentration from 13.5 – 15 % (w/v).

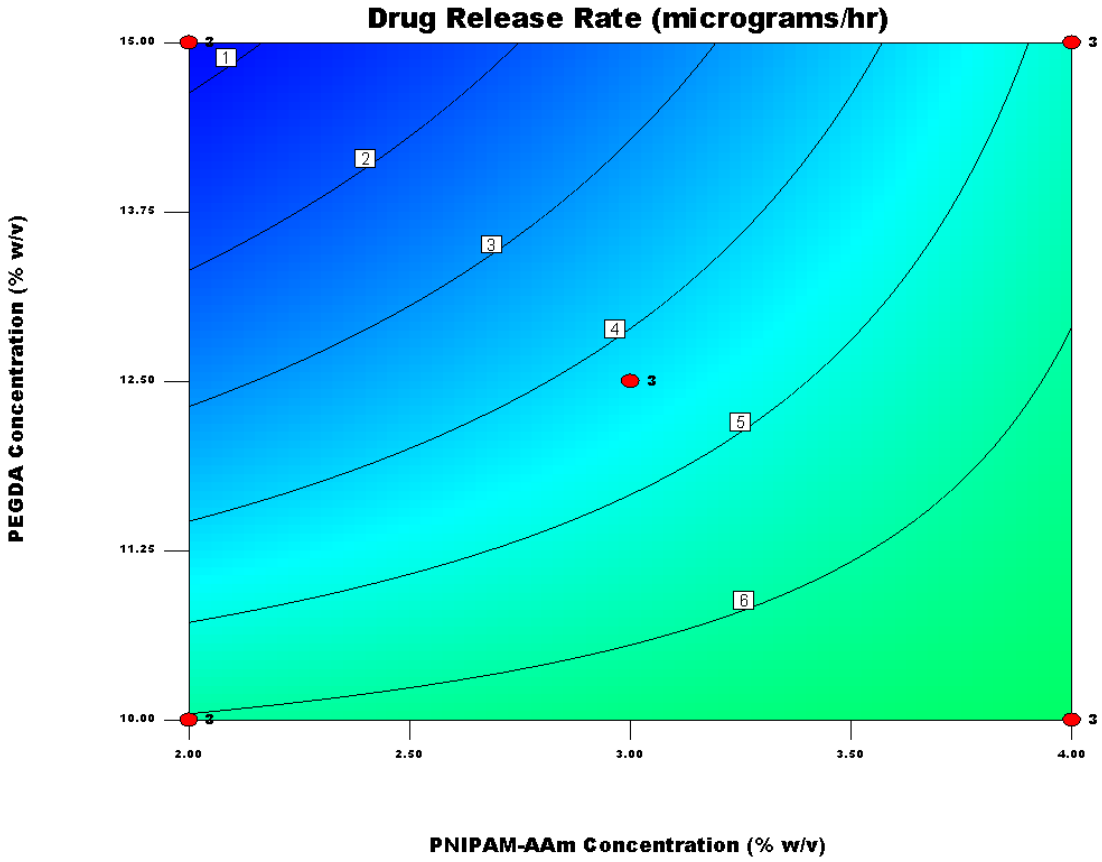

Figure 4.3 Contour plot for protein release rate from slit geometry during 1st OFF cycle.

Cross:

The equation for protein release rate from the cross geometry during the 1st OFF cycle in terms of actual factors and combined effect of factors is given below.

$$\mathbf{R \text{ for } 1^{st} \text{ OFF cycle } (\mu g/hr) = [(3.74096 + (0.20531)N - (0.11595)P + (0.015569)NP]^2}$$

Where R is the protein release rate, N is the PNIPAM-AAm concentration, P is the PEGDA concentration. It is evident that there is an antagonistic interaction between increased PNIPAM-AAM concentration and

lower PEGDA concentration which results in higher protein release rates in the off cycles primarily by a diffusion driven process.

Figure 4.4 shows the surface response diagram for the protein release rate during the 1st OFF cycle for the cross geometry.

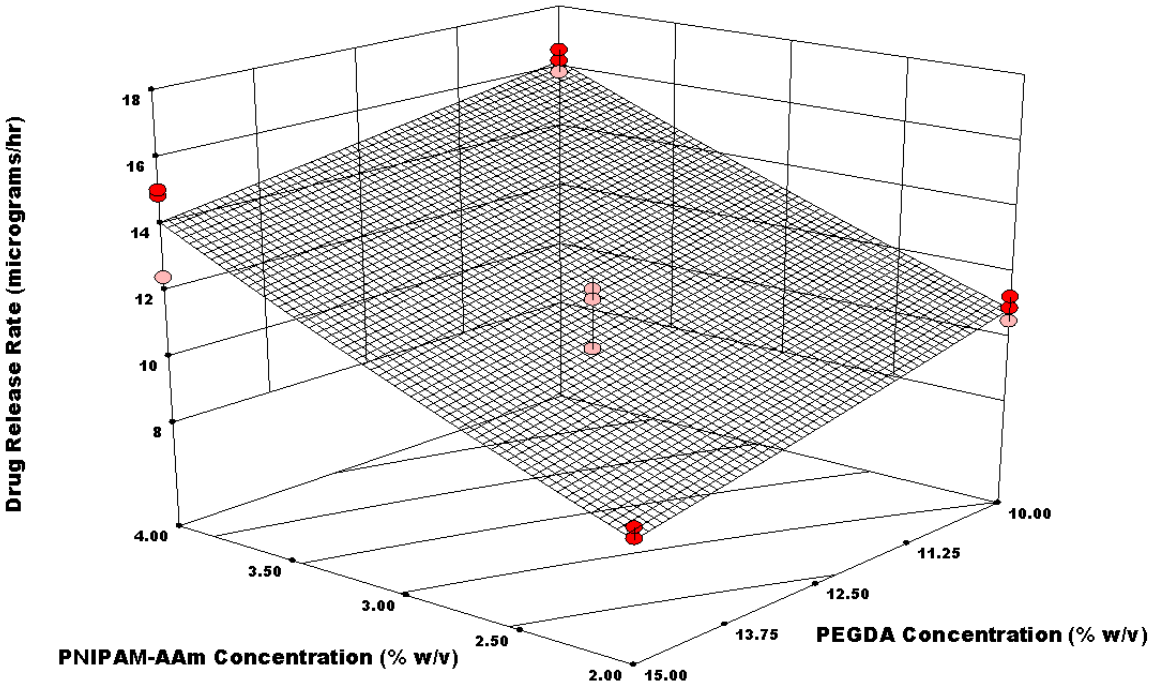

Figure 4.4 Response surface diagram for cross geometry during 1st OFF cycle.

As can be seen in Figure 4.4, the protein release in the 1st OFF cycle is much more dependent on the PNIPAM-AAm concentration than on the PEGDA concentration for the cross geometry. In addition, comparison of Figure 4.2 and 4.4 it is evident that the cross geometry has a higher protein release rate in the 1st off cycle compared to the slit geometry. At a higher PNIPAM-AAm concentration, increasing the PEGDA concentration does has a marginal negative effect similar to lowering the PNIPAM-AAm

concentration. The release rates are in the range of 8-16 µg/hr. The actual midpoint values lie slightly below the predicted response surface as opposed to the slit design where the midpoint values are higher than the predicted ones.

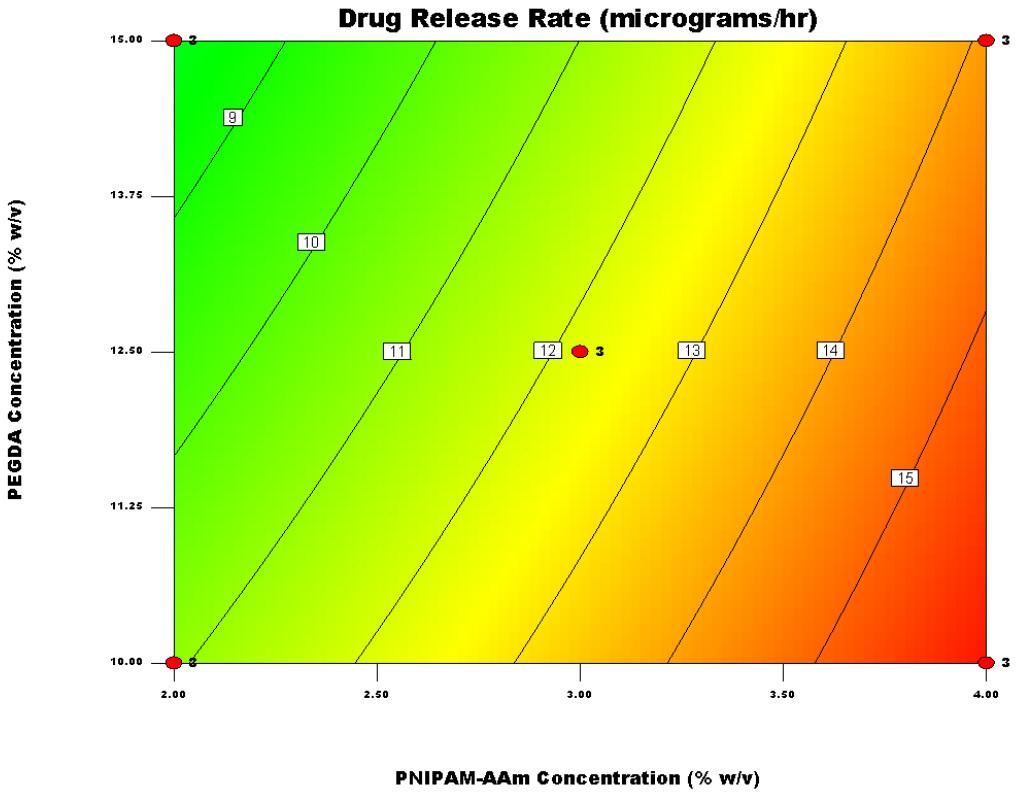

Figure 4.5 Contour plot for release rate during 1st OFF cycle from cross geometry

The orientation of the contours of iso-protein release rate from the cross geometry in Figure 4.5 indicates that increasing protein release is associated with increased PNIPAM-AAm concentration and lower PEGDA concentration.

Discussion:

During the 1st OFF cycle, the hydrogels are maintained at 23.1 ℃, which is below the LCST. The protein release here is primarily due to diffusion of proteins through the swollen hydrogel and out through

the device geometry. Thus, it is understood that the device geometry is the most significant limiting factor for the protein release. The protein release rate for the slit geometry is less than that for the cross geometry during the 1st OFF cycle. Since the effective surface area of both the geometries are the same (5 mm^2), the seal provided by the swollen hydrogel must be more effective for the slit geometry in comparison to the cross geometry. While the PNIPAM-AAm concentration and PEGDA concentrations have an antagonistic effect on the protein release rate for the slit geometry, the protein release rates are more dependent on the nanoparticle concentration for the cross geometry. The protein release rates are more or less linearly dependant on the nanoparticle and polymer concentration for the cross geometry.

4.4.2 First ON Cycle

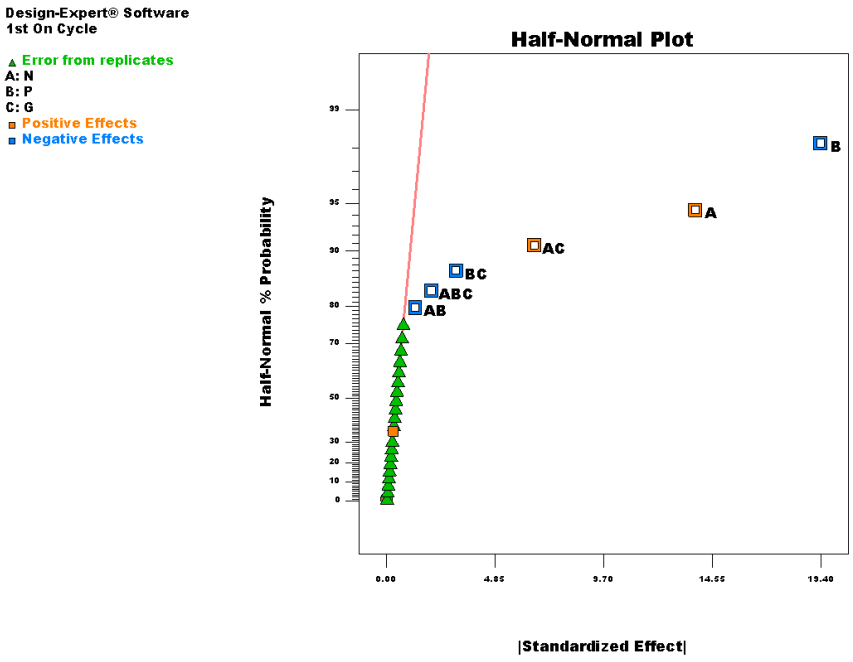

Figure 4.6 Half normal plot for 1st ON cycle where A: N stands for PNIPAM-AAm, B: P stands for PEGDA and G stands for geometry of the device.

From the half normal plot shown in Figure 4.6, the PEGDA concentration is shown to have the most significant effect (negative) on the protein release rate during the 1st OFF cycle, followed by the PNIPAM-AAm concentration (positive effect). A combination of the PNIPAM-AAm concentration and

device geometry interaction also has a positive effect on the protein release behavior. The remaining factors lie close to the zero line and can be ignored.

A look at the response surface diagrams for the slit and cross geometries gives insight on the protein release behavior during the 1st ON cycle.

Slit:

The equation for protein release rate from the slit geometry during the 1st ON cycle in terms of actual factors and combined effect of factors is given below.

R for 1st On Cycle (µg/hr) = 64.80300 + (18.44550) N - (2.52320) P - (0.65920) NP

Where R is the protein release rate, N is the PNIPAM-AAm concentration, P is the PEGDA concentration.

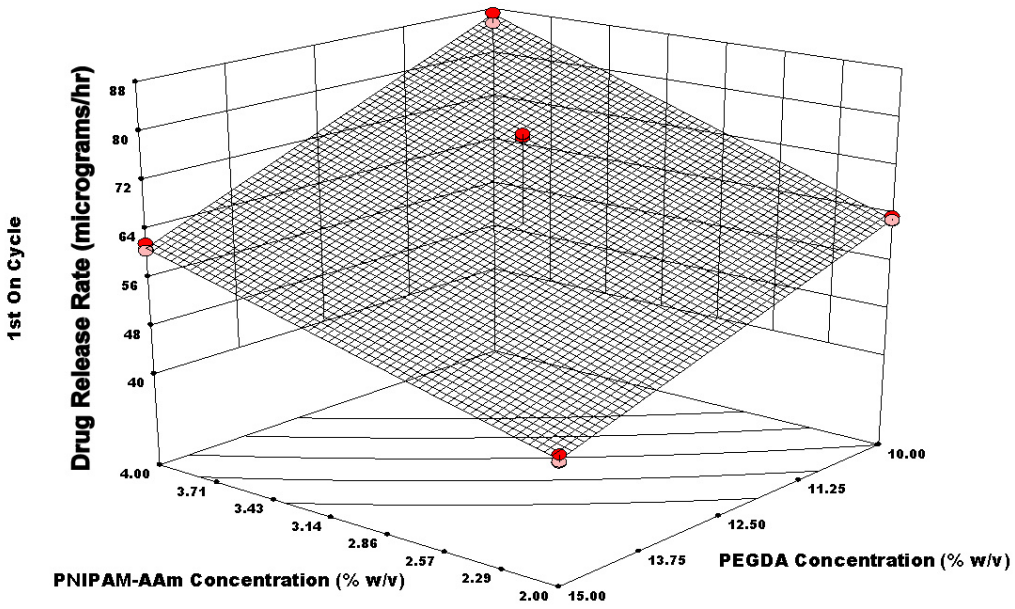

Figure 4.7 Response surface diagram for slit geometry during 1st ON cycle showing the protein release rate as a function of PNIPAM-AAm and PEGDA concentrations.

Figure 4.7 shows the response surface diagram for protein release from the slit geometry during the 1st ON cycle. The PEGDA concentration and PNIPAM-AAm concentration have a strong effect on the protein release rate during this cycle. At 2% (w/v) PNIPAM-AAm and 10% (w/v) PEGDA concentration, the release rates are similar to when 4% (w/v) PNIPAM-AAm and 15% (w/v) concentration. There is an inverse synergistic/antagonistic effect between the PEGDA and PNIPAM-AAm concentration on protein release rates. The highest release rate of BSA occurs when PEGDA concentration is lowest and PNIPAM-AAm concentration is the highest and the lowest release rate of BSA occurs when PEGDA concentration is highest and PNIPAM-AAm concentration is highest. The positive effect of the PNIPAM-AAm concentration is countered by the negative effect of the PEGDA concentration. This relationship is seen more clearly in the contour plot in Figure 4.8 below.

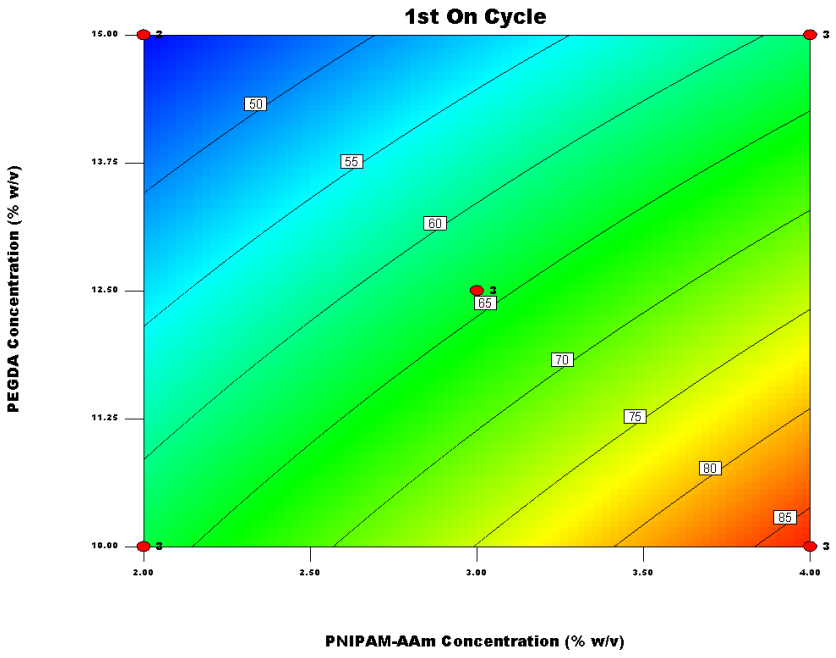

Figure 4.8 Contour plot for protein release rate from slit geometry during 1st ON cycle. Iso-protein release rates are in µg/hr. Release rates increase with increasing PNIPAM-AAm concentration and decreasing PEGDA concentration.

Cross:

The equation for protein release rate from the cross geometry during the 1st ON cycle in terms of actual factors and combined effect of factors is given below.

R for 1st On Cycle (µg/hr) = 98.93459 + (1.78952) N – (3.69286) P + (0.14477) NP

Where R is the protein release rate, N is the PNIPAM-AAm concentration, P is the PEGDA concentration.

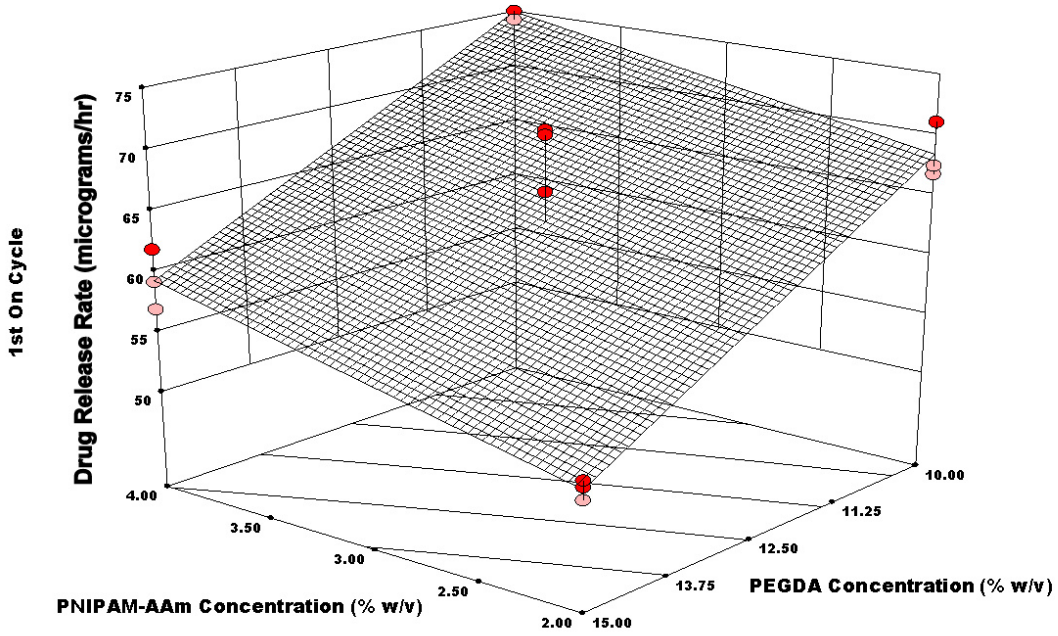

Figure 4.9 Response surface diagram for cross geometry during 1st ON cycle for release rates in µg/hr as a function of PNIPAM-AAm concentration and PEGDA concentration.

Figure 4.9 above is the response surface diagram of the protein release rate from the cross geometry during the 1st ON cycle. Unlike the slit geometry the cross geometry does not exhibit equi-release rate profile for the 10% PEGDA/2% PNIPAM-AAm and 15% PEGDA/4% PNIPAM-AAm, the PEGDA plays a larger role in the cross geometry with high concentrations resulting in lower BSA release

rate. However, overall the RSD indicates a flatter response over the range of concentration in the Cross geometry as the lowest and highest release rate for the 15% PEGDA/2% PNIPAM-AAm at 50 µg/hr and 10% PEGDA/4% PNIPAM-AAm at 75 µg/hr are closer together in the cross than in the case of the slit which ranges from 40 to 88 µg/hr respectively. The PEGDA concentration has a more significant effect (negative) on the release rate when compared to the PNIPAM-AAm concentration effect. At 10% (w/v) PEGDA (low level) and 2% (w/v) PNIPAM-AAm concentration (low level), the release rate is higher in comparison to the release rate at 15% (w/v) PEGDA (high level) and 4% (w/v) PNIPAM-AAm concentration (high level). From the contour plot of the protein release rate in Figure 4.10 below, the protein release rate can be said to have a linear relationship with the PEGDA and PNIPAM-AAm concentration.

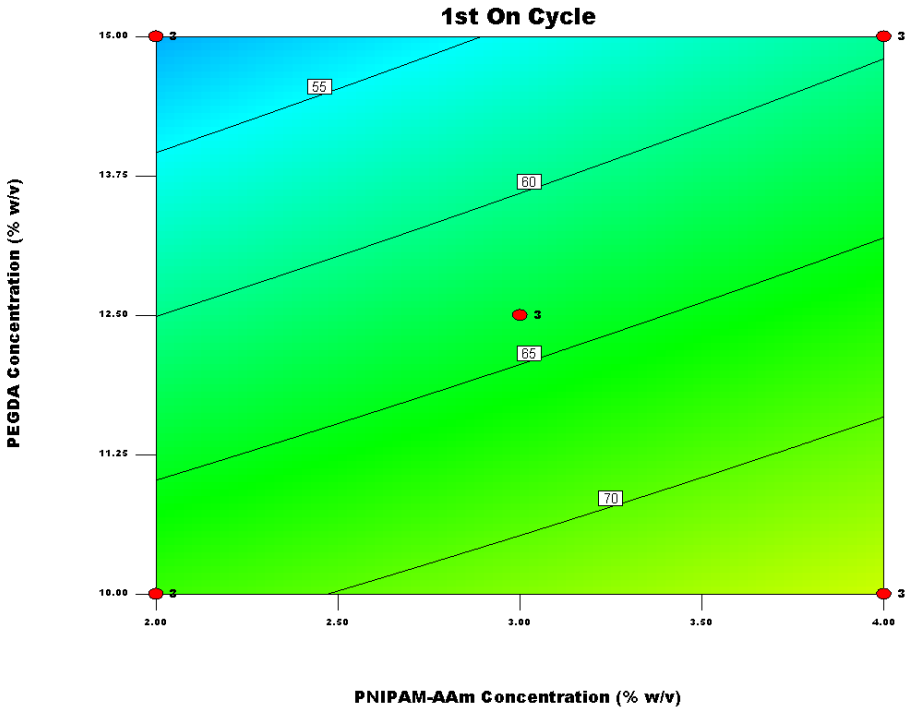

Figure 4.10 Contour plot for protein release rate from cross geometry during 1st ON cycle. Iso-protein release rates are in µg/hr. Release rates decrease with increasing PEGDA concentration.

Discussion:

During the 1st ON cycle, the hydrogel is maintained at 41 ℃ (abo ve the LCST), thus it is in its shrunken state, increasing the free volume inside the device cavity for the expelled water and protein to escape from the device opening. Comparable release rates were observed for both the slit and cross geometries, and a linear relationship was observed between the protein release rate and the PEGDA concentration (inverse relationship) and PNIPAM-AAm (direct relationship) for both the geometries. However, for the slit geometry, the two factors countered each other's effect in a more balanced manner, suggesting that both had equal significance on the protein release rate. The PEGDA concentration proved to have a more important impact on the protein release rate in case of the cross geometry.

4.4.3 Second OFF Cycle

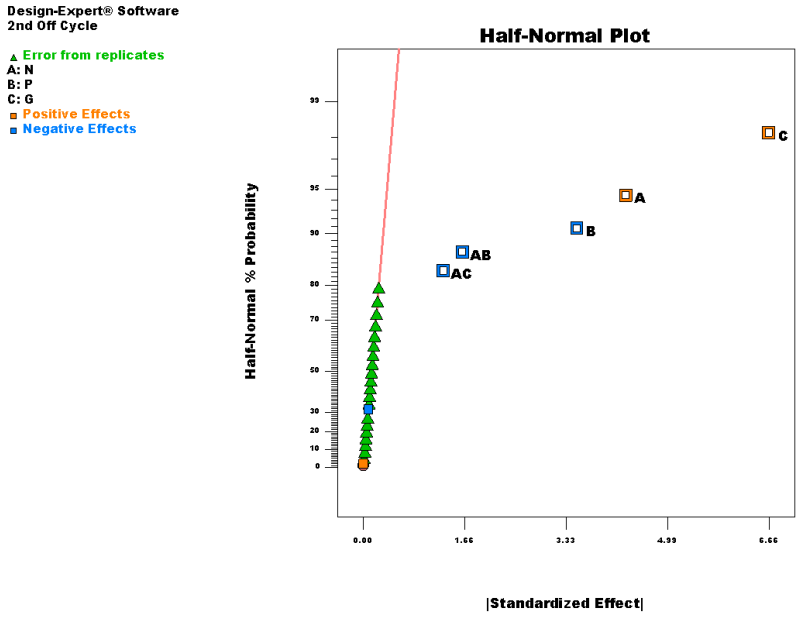

Figure 4.11 Half normal plot for 2nd OFF cycle A (N) corresponds to the PNIPAM-AAM, B (P) corresponds to PEGDA and G corresponds to the device geometry (slit or cross).

During the 2nd OFF cycle, the device geometry plays the most important role controlling the protein release rate. It has a positive effect on the release rate, thus the choice of the right geometry

factor is critical in the design. The PNIPAM-AAM concentration (positive effect) and PEGDA concentration (negative effect) also have a significant effect on the release rate followed by the combined two-factor interactions of PNIPAM-AAm and PEGDA concentrations as well as PNIPAM-AAm concentration and geometry, both of which have negative effect on the protein release rate.

Slit:

The equation for protein release rate from the slit geometry during the 2nd OFF cycle in terms of actual factors and combined effect of factors is given below.

R for 2nd OFF Cycle (µg/hr) = 8.28683 + (5.56646) N + (0.27560) P – (0.32562) NP

Where R is the protein release rate, N is the PNIPAM-AAm concentration, P is the PEGDA concentration.

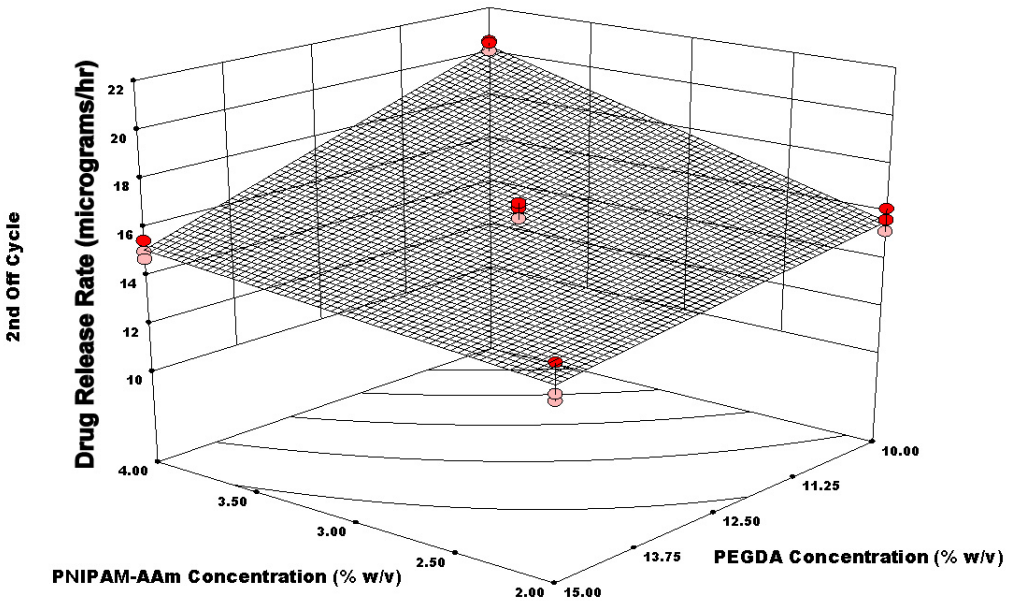

Figure 4.12 Response surface diagram for slit geometry during 2nd OFF cycle showing release rate (µg/hr) as a function of PNIPAM-AAm and PEGDA concentration.

Figure 4.12 is the response surface diagram of the release rate from the slit geometry during the 2nd OFF cycle. As can be seen from the diagram, the protein release rate is not too sensitive to changes in the PNIPAM-AAm concentration and PEGDA concentration, however, the same trends regarding the inverse variance with PEGDA concentration and direct variance with PNIPAM-AAm concentration seen for all the cycles are seen. During the OFF cycle, the geometry becomes the most important controlling factor for protein release. There is a mild inverse synergistic effect between the PNIPAM-AAm concentration and PEGDA concentration on release rate during the off cycle with the highest release for the lowest PEGDA concentration and highest PNIPAM-AAm concentration and vice-versa. The range between the lowest and highest rate of release lies between 11 and 20 µg/hr at the extremes.

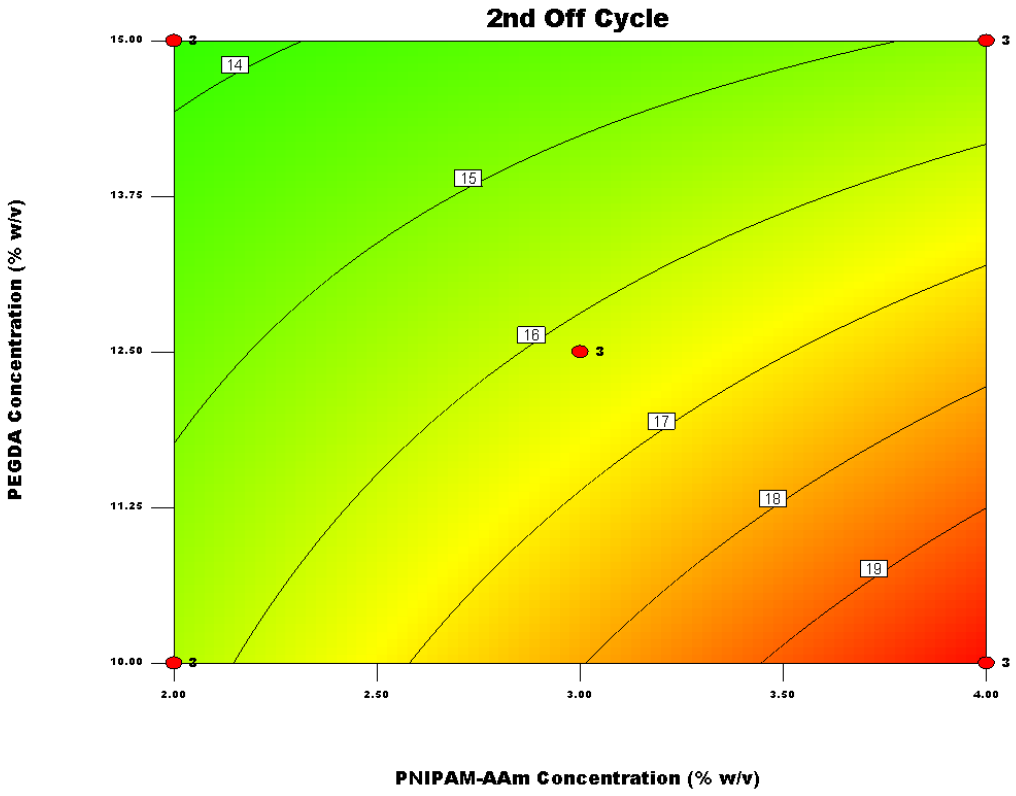

Figure 4.13 Contour plot for protein release rate from slit geometry during 2nd OFF cycle. Iso-protein release rates increase with increasing PNIPAM-AAm concentration and decreasing PEGDA concentration.

Figure 4.13 displays the contour plot for the protein release rate. The release rates have an inverse relationship between PNIPAAM-AAm and PEGDA concentration. To retain the same release rate during the off cycle, the concentration of PNIPAM-AAm has to be increased with an increase in PEGDA concentration to maintain iso-release rates. .

Cross:

The equation for protein release rate from the cross geometry during the 2nd OFF cycle in terms of actual factors and combined effect of factors is given below.

R for 2nd OFF Cycle (µg/hr) = - 2.31483 + (6.88187) N + (0.27560) P – (0.32562) NP

Where R is the protein release rate, N is the PNIPAM-AAm concentration, P is the PEGDA concentration.

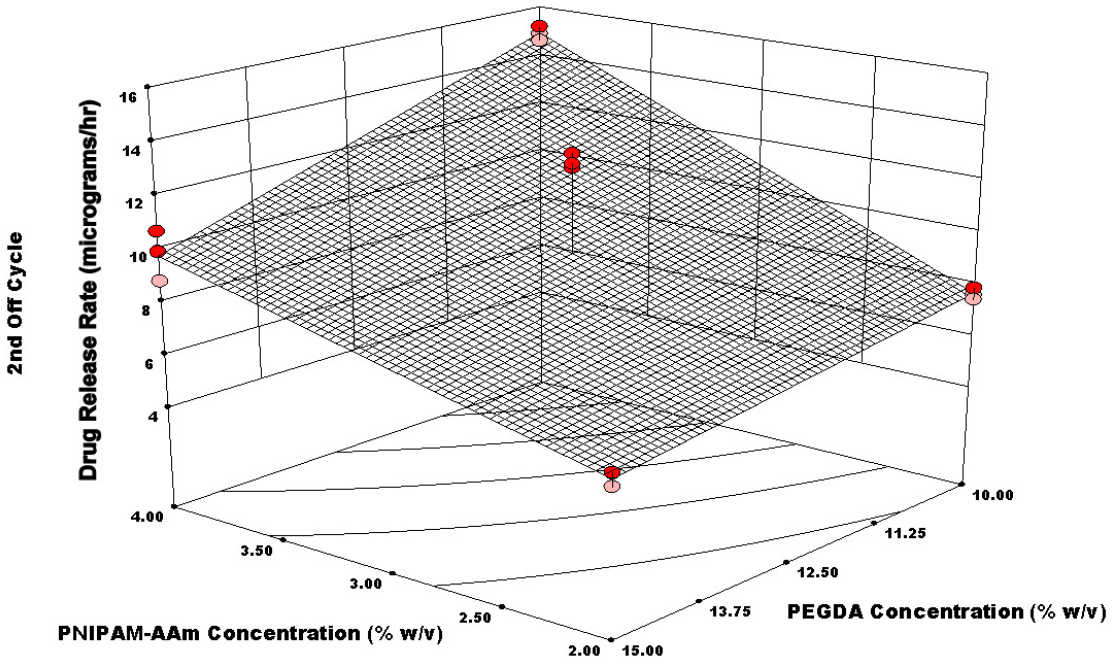

Figure 4.14 Response surface diagram for cross geometry during 2nd OFF cycle release rate (µg/hr) as a function of PNIPAM-AAm and PEGDA concentration.

As can be seen from the response surface diagram shown in Figure 4.14, for low values of PEGDA concentration, the PNIPAM-AAm concentration is the most significant factor affecting protein release. Even at high PEGDA concentration (negative effect) and corresponding high PNIPAM-AAm concentration, the release is higher than the opposite conditions graphically located diagonally across. The highest release rate is approximately 15 µg/hr, when at the lower level of PEGDA and higher level of PNIPAM-AAm concentration, respectively. In comparison the slit geometry, the lowest release rate in the off cycle is 14 µg/hr at the lowest PNIPAM-AAm concentration and highest PEGDA concentration. It is clear that during the off cycle, the cross geometry is much more efficient in holding the BSA within the device compared to the slit geometry while during the first ON cycle the release rates are comparable.

Figure 4.15 shows the contour plot of the release rates from the cross geometry during the 2nd OFF cycle.

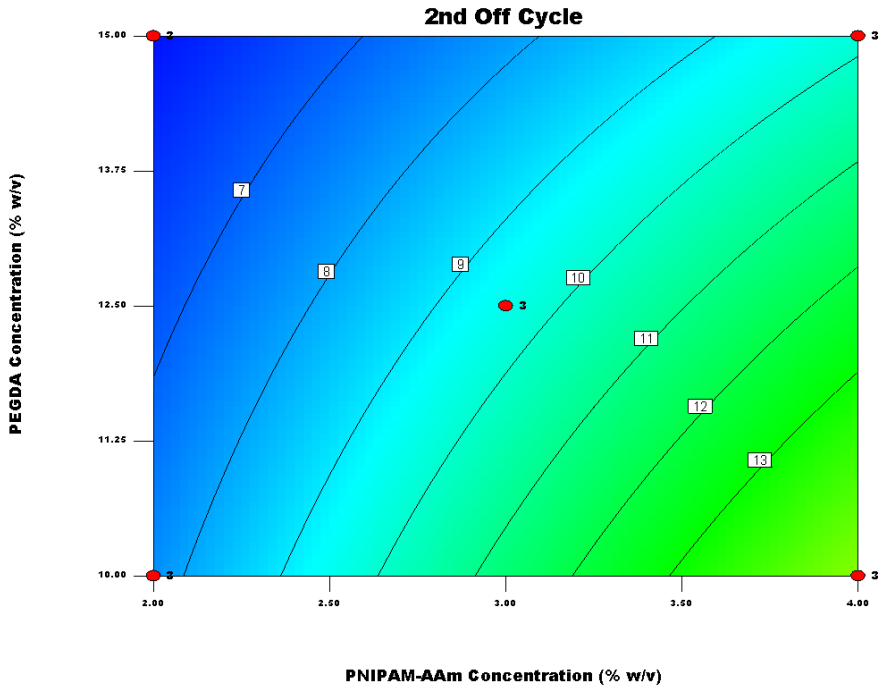

Figure 4.15 Contour plot for protein release rate from cross geometry during 2nd OFF cycle. Increasing PNIPAM-AAm concentration increases the protein release rates, but the degree of increase is small.

The contours resemble a hill-side response, with increasing linear dependence with increasing PNIPAM-AAm concentration. Even though the general trend is a decreased release rate with increase in PEGDA concentration, a PEGDA concentration as low as 11.75% (w/v) and as high as 15% (w/v) for corresponding 2% (w/v) PNIPAM-AAm nanoparticle concentration results in the same constant release rate response of 7 µg/hr.

Discussion:

The release rates during the 2nd OFF cycle are greater than those observed for the 1st OFF cycle. This can be because the all the protein released during the 1st ON cycle may not have escaped through the device geometry. Some of the protein released may have adhered to the surface of the hydrogel, rather than being trapped in the hydrogel network during subsequent re-swelling in the 2nd OFF cycle. Diffusion out of the device geometry of protein molecules present on the surface is much easier than those entrapped in the hydrogel network. Thus, obviously, the device geometry plays the most significant role in controlling the release rates during this cycle. The release rates are more dependent on the PEGDA concentration for the cross geometry than for the slit geometry. As the PNIPAM-AAm concentration increases, the release response becomes more linear. In addition, the cross geometry has a significantly lower release rate of the BSA during the 2nd off cycle in comparison to the slit geometry.

4.4.4 Second ON Cycle

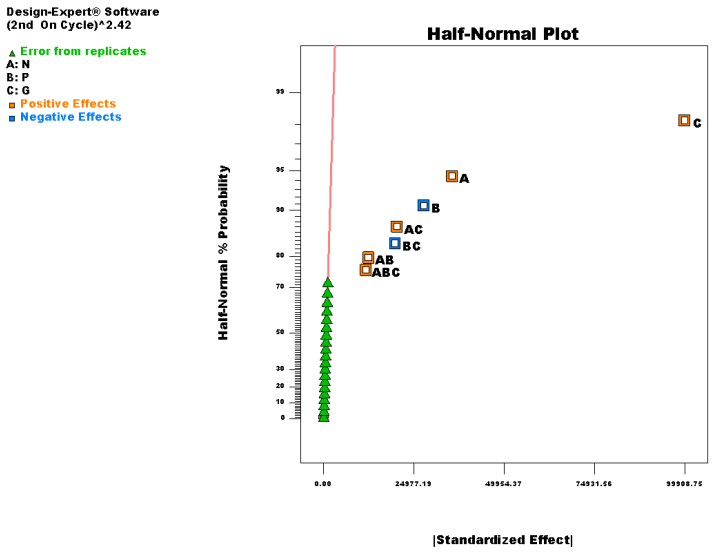

Figure 4.16 Half normal plot for 2nd ON cycle A (N) corresponds to the PNIPAM-AAM, B (P) corresponds to PEGDA and G corresponds to the device geometry (slit or cross).

Figure 4.16 displays the half normal plot for the effect of PNIPAM-AAm and PEGDA concentration on the protein release rate during the 2nd ON cycle. The geometry has the most significant effect on the response. The PNIPAM-AAm concentration and PEGDA concentration have relatively less importance on the release rate, and even lesser contributions made by the two and three-factor interactions.

Slit:

The equation for protein release rate from the slit geometry during the 2nd OFF cycle in terms of actual factors and combined effect of factors is given below.

R for 2nd ON Cycle (µg/hr) = [(3.44919E+005) – (32402.05239) N – (23983.30628) P + (4828.22637) NP] $^{0.4132}$

Where R is the protein release rate, N is the PNIPAM-AAm concentration, P is the PEGDA concentration.

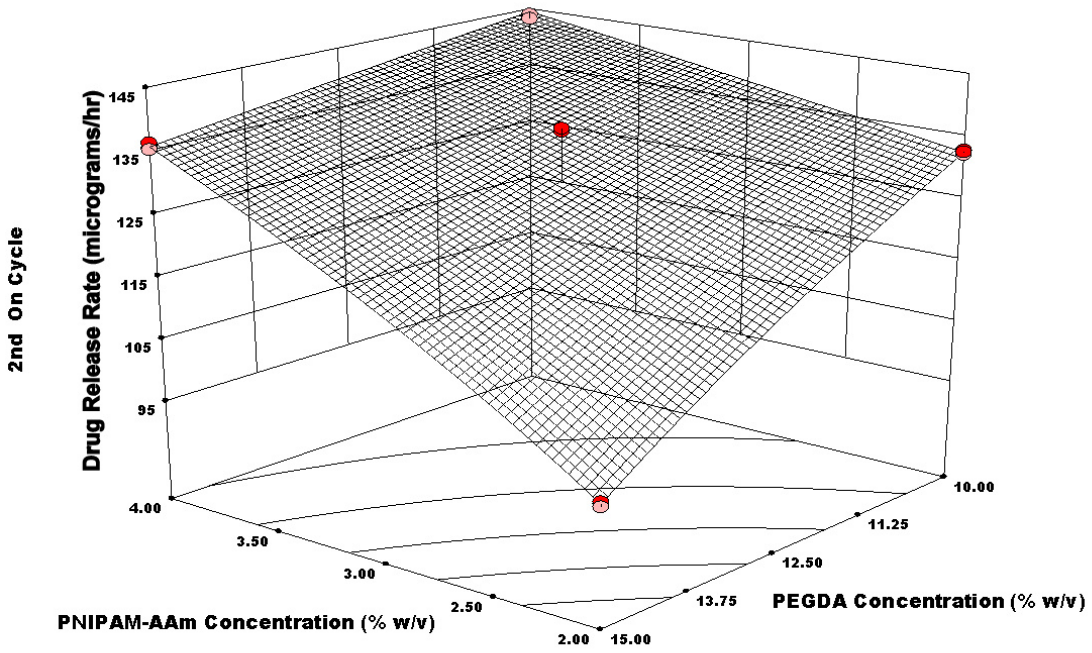

Figure 4.17 Response surface diagram for slit geometry during 2nd ON cycle release rate (µg/hr) as a function of PNIPAM-AAm and PEGDA concentration.

From Figure 4.17, we see that the increasing PEGDA concentration and decreasing PNIPAM-AAm concentration have an antagonistic effect on the protein release rate from the slit geometry in the 2nd ON cycle. The dependence of the release rate on the two factors is not linear. The release rates drop significantly when the PEGDA concentration is high and PNIPAM-AAm nanoparticle concentration is low. However, either increasing the PNIPAM-AAm concentration and/or decreasing the PEGDA concentration improves the release rate. The release rate in the second ON cycle for the slit geometry can be modulated between 95 and 145 µg/hr compared to a range of 40 to 88 µg/hr in the first ON cycle for slit geometry while the release rate in the 2nd OFF cycle ranges between 10-20 µg/hr. This clearly indicates

that we are able to modulate the release rate of the protein during the ON and OFF cycles. It is also evident that during the OFF cycle following an ON cycle, much of the drug is recaptured within the hydrogel, however, the binding efficiency of the BSA to the PNIPAM-AAm is weakened resulting in a faster release in the second ON cycle compared to the first cycle.

Figure 4.18 presents the protein release rate contours for the slit geometry during the 2nd ON cycle.

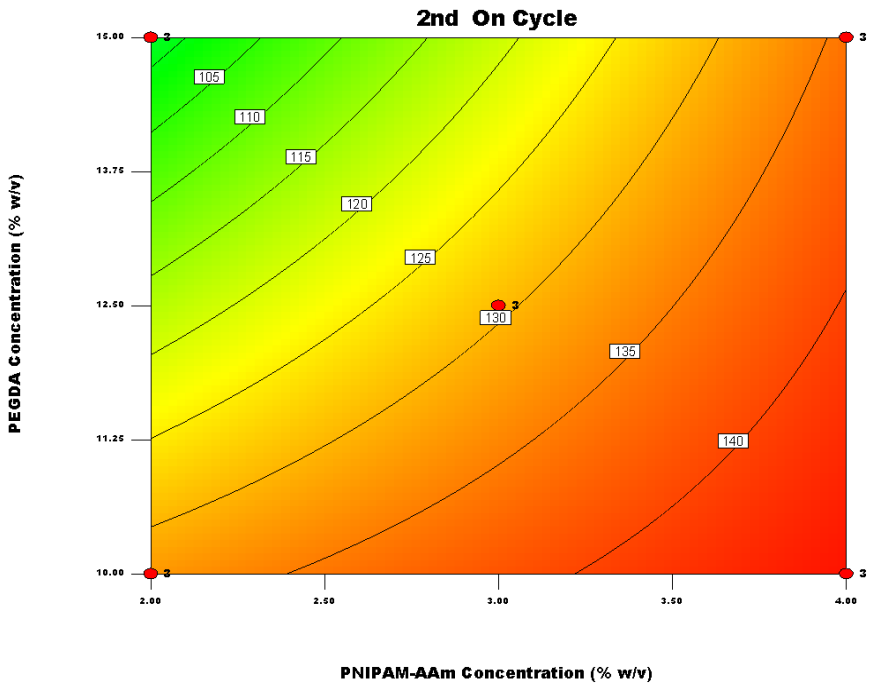

Figure 4.18 Contour plot for protein release rate from slit geometry during 2nd ON cycle. Iso contour lines in terms of µg/hr.

The contour plots illustrates the results of the RSD and clearly indicate the dependence of the PNIPAM-AAm and PEGDA concentration on the release rate.

Cross:

The equation for protein release rate from the cross geometry during the 2nd OFF cycle in terms of actual factors and combined effect of factors is given below.

R for 2nd ON Cycle (µg/hr) = [31638.91318 + (5753.94487) N – (2030.95306) P + (148.20276) NP] $^{0.4132}$

Where R is the protein release rate, N is the PNIPAM-AAm concentration, P is the PEGDA concentration.

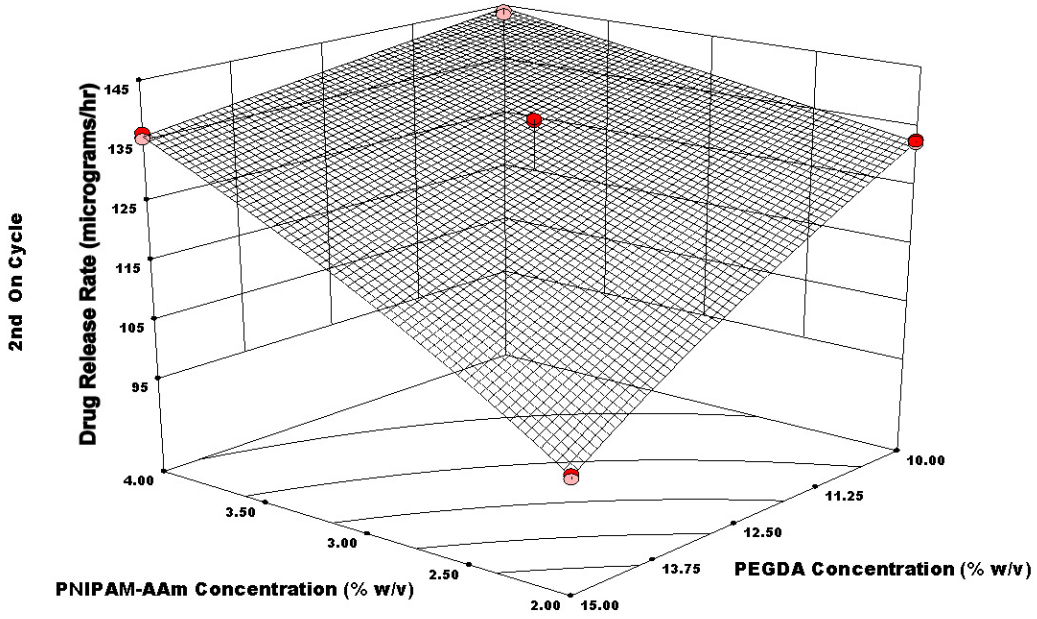

Figure 4.19 Response surface diagram for cross geometry during 2nd ON cycle release rate (µg/hr) as a function of PNIPAM-AAm and PEGDA concentration.

Figure 4.19 tells us that the PNIPAM-AAm concentration plays a greater role in controlling the release rate than the PEGDA concentration. Increasing the PNIPAM-AAm concentration even at a high PEGDA concentration (negative effect), increases the release rate by almost 30 µg/hr. The actual

midpoint release rate values lie much below the predicted values. Increasing the number of runs at different levels may lead to a better fit of the surface curve.

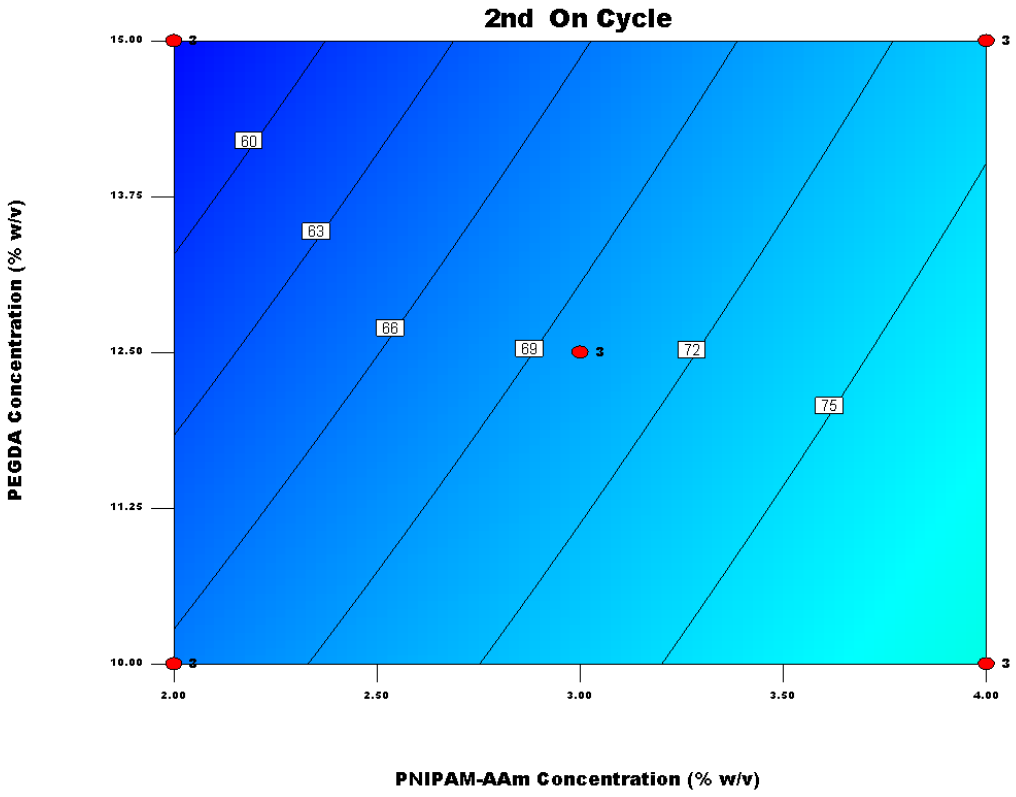

Figure 4.20 Contour plot for protein release rate from cross geometry during 2nd ON cycle. Iso-release rates in µg/hr.

Figure 4.20 is a contour plot of iso-release rate plotted as a function of PEGDA and PNIPAM-AAm concentration. The 45° angle of the plots indic ate a inverse relationship between PEGDA and PNIPAAM-AAm concentration as far as BSA release rate for the cross geometry is concerned.

Discussion:

The release rate response varies greatly with the two geometries. While the slit geometry has a rapid increase in BSA release with increasing PNIPAM-AAm concentration and decreasing PEGDA concentration, the dependence is larger on the PNIPAM-AAm concentration in the case of the cross

geometry. However, the overall release rates are much higher for the slit geometry in comparison with the cross geometries suggesting that the longer slit geometry reached closer to the edges of the device resulting in greater release of BSA.

4.4.5 First ON Cycle during Steady State Release

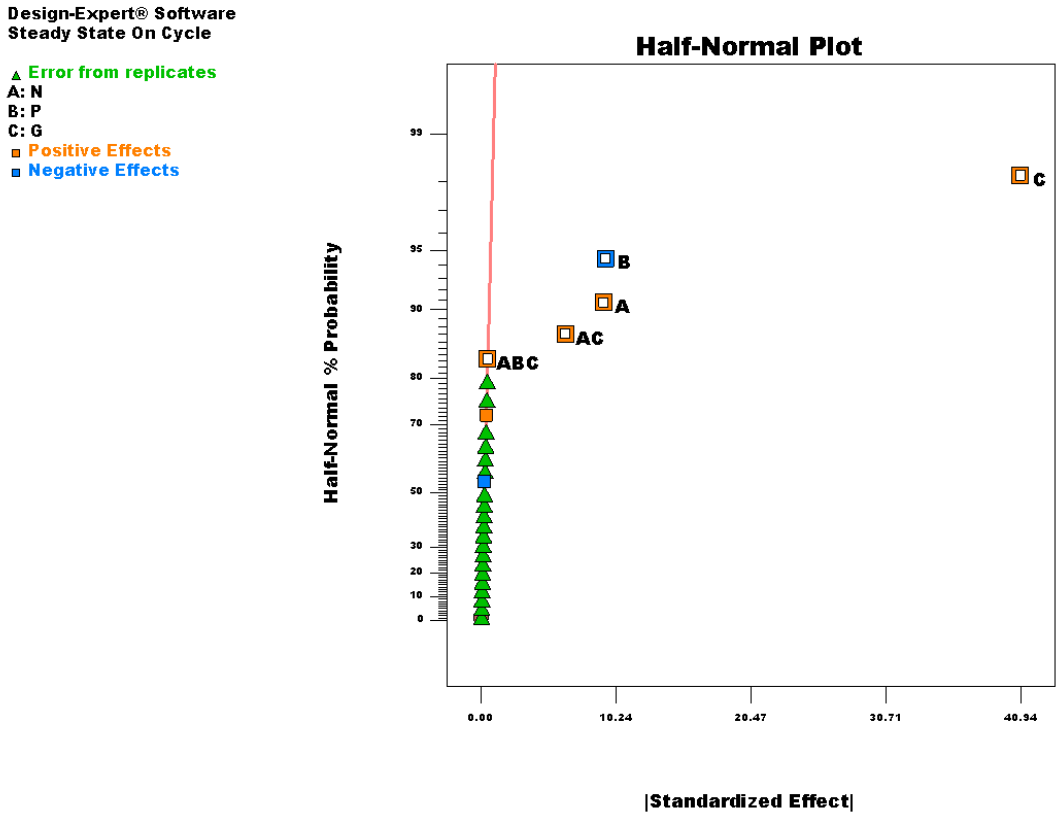

Figure 4.21 Half normal plot for steady state ON cycle A (N) corresponds to the PNIPAM-AAM, B (P) corresponds to PEGDA and G corresponds to the device geometry (slit or cross).

Steady state release is that part of the release curve where subsequent thermal cycling results in constant release rates for the ON and OFF cycles. Figure 4.21 depicts the half normal plot for the effect of device geometry, PNIPAM-AAm concentration and PEGDA concentration on the release rate during the first steady state release cycle. The device geometry has the most significant effect on the release rate during this cycle. The PEGDA and PNIPAM-AAm concentrations have an almost equal negative and

positive effect on the release rate. The combined effect of device geometry and PNIPAM-AAm concentration also has a slight positive effect on the response.

Slit:

The equation for protein release rate from the slit geometry during the steady state cycle in terms of actual factors and combined effect of factors is given below.

R for Steady State ON Cycle (µg/hr) = 77.82633 + (7.27750) N – (1.95180) P + (0.046867) NP

Where R is the protein release rate, N is the PNIPAM-AAm concentration, P is the PEGDA concentration.

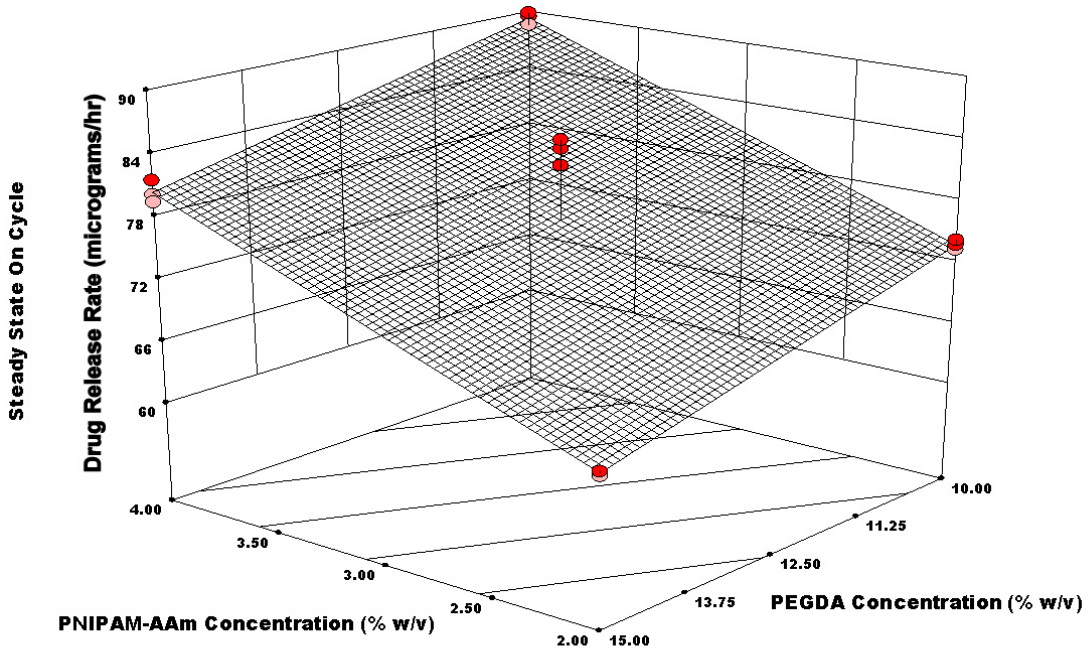

Figure 4.22 Response surface diagram for slit geometry during steady state release rate (µg/hr) as a function of PNIPAM-AAm and PEGDA concentration.

As can be seen, the release rate values have come down from the corresponding release rate values observed during the 2nd ON cycle. For the slit geometry, the release response is more dependent on the PNIPAM-AAm concentration than the PEGDA concentration. This also is seen in the fact that the release rate for high levels of PEGDA (inverse variance with response) and PNIPAM-AAm (direct variance with response) is higher than that for low levels of the same factors. The response surface appears to be planar; however, the actual midpoint release rates are higher than those predicted by the model.

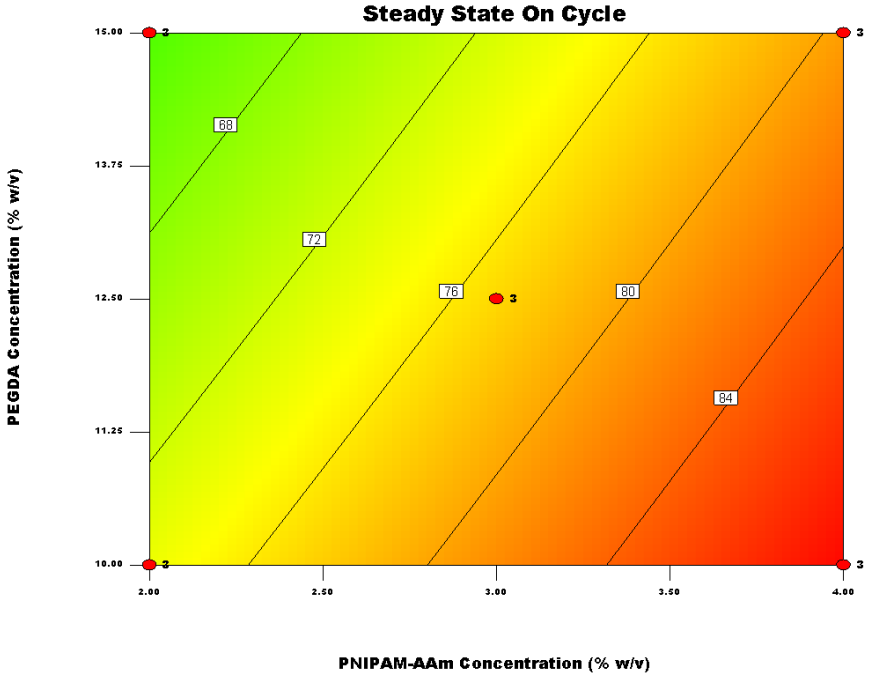

Figure 4.23 Contour plot for protein release rate from slit geometry during steady state ON cycle. Iso release rates in µg/hr. A linear profile of release rates is observed.

A linear relationship is evident; the response is more sensitive to the changes in the PNIPAM-AAm concentration.

Cross:

The equation for protein release rate from the cross geometry during the 2nd OFF cycle in terms of actual factors and combined effect of factors is given below.

R for Steady State ON Cycle (µg/hr) = 50.74340 + (3.33390) N – (1.52203) P – (0.15053) NP

Where R is the protein release rate, N is the PNIPAM-AAm concentration, P is the PEGDA concentration.

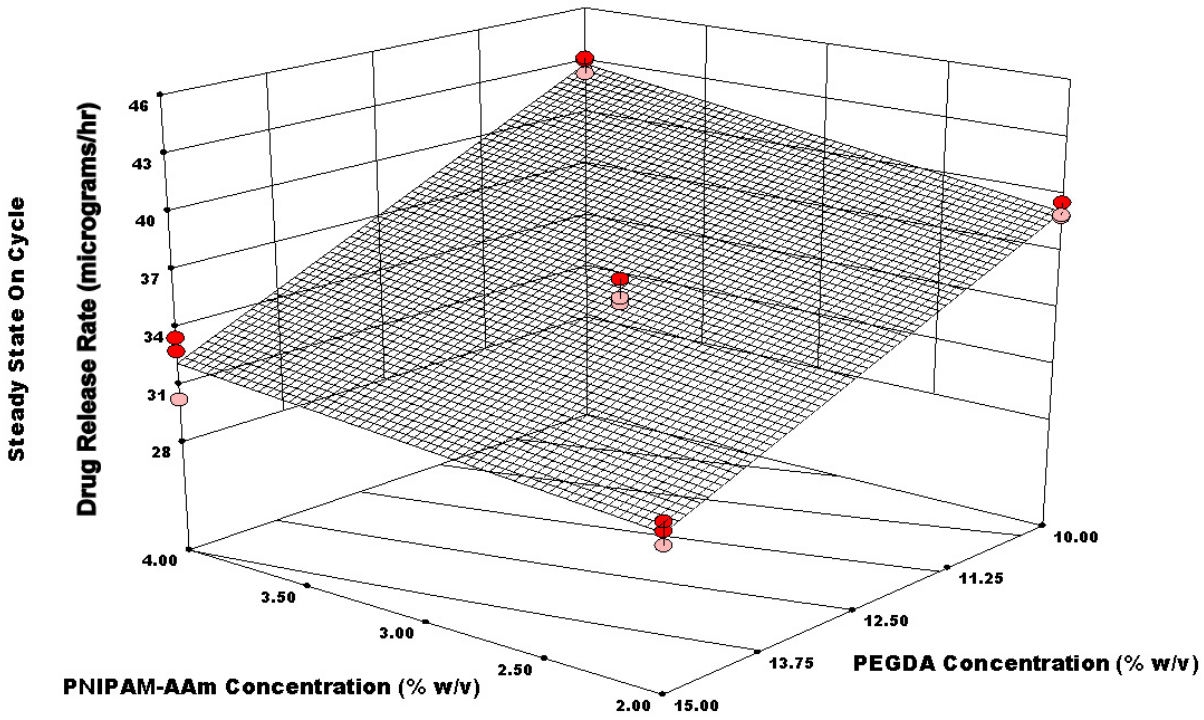

Figure 4.24 Response surface diagram for cross geometry during steady state release rate (µg/hr) as a function of PNIPAM-AAm and PEGDA concentration.

Figure 4.24 displays the response surface diagram for protein release rate from the cross geometry during the 1st ON cycle of steady state release. The response is clearly more dependent on the

PEGDA concentration, with the rate decreasing by 10 µg/hr when the PEGDA concentration is increased from 10% (w/v) to 15% (w/v). The release rate for high levels of both the factors is much less than that for low levels, confirming the dominant effect of the PEGDA concentration on the release rate. The actual midpoint release rates lay close to the predicted response surface, thus the model is a good fit. In addition a comparison of Fig. 4.24 and 4.22 clearly indicates that the rate of BSA release with the cross geometry is much slower than the slit geometry and one can modulate the release better with the cross than the slit geometry.

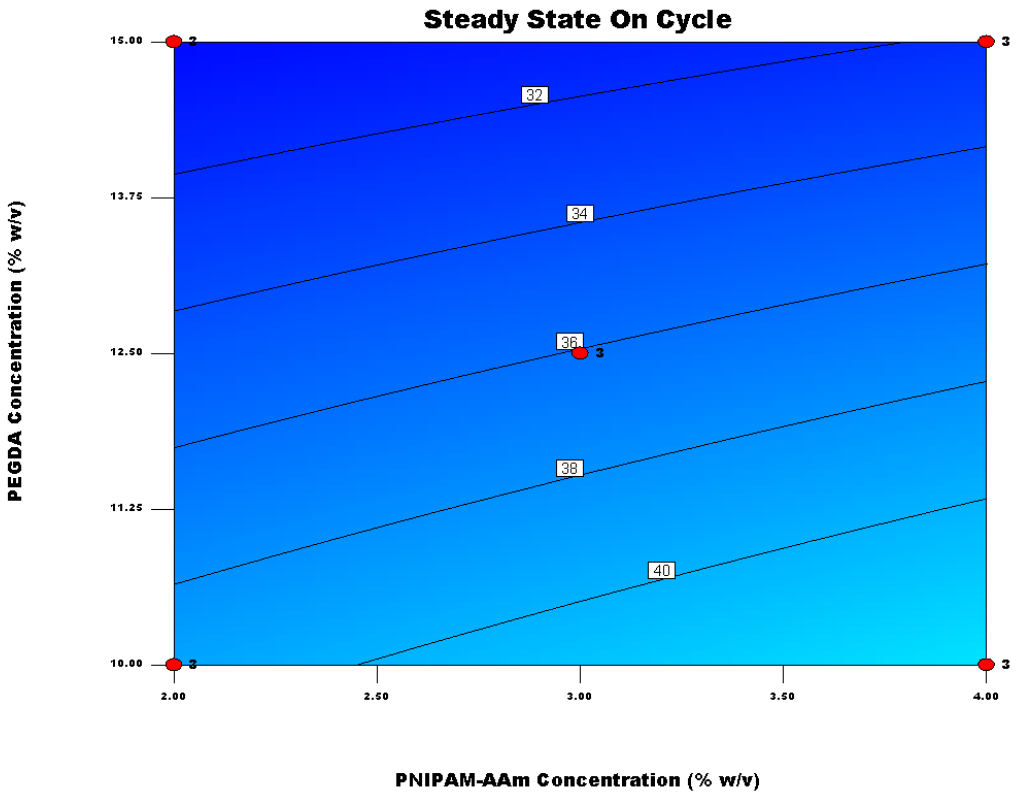

Figure 4.25 Contour plot for protein release rate from cross geometry during steady state ON cycle. The iso-contour lines are in µg/hr and show a greater dependence of the release rates on the PEGDA concentration.

From Figure 4.25, it is very clear that the PEGDA cocentration is the controlling factor in the protein release rate response. The contour steps are equally spaced, signifying a steady increase in release rate with decrease in PEGDA concentration.

Discussion*:*

A clear differentiation between the release rate dependence on the device geometries is observed during the steady state ON release cycle. While the PNIPAM-AAm concentration plays a more significant role in controlling the protein release for the slit geometry, the PEGDA concentration plays a more significant role in controlling the response for the cross geometry. The release rates have a higher range of values for the slit geometry. Both the geometries have a steady linear response though.

4.4.6 Cumulative Protein Release

Figure 4.26 provides the half-normal plot for the effect of PNIPAM-AAm concentration, PEGDA concentration and device geometry on the cumulative protein released over 24 hours of thermal cycling. The device geometry has the most significant effect, followed by the nanoparticle concentration, both of which have a direct variance with the response. The PEGDA concentration has a negative effect, and to some extent so does the two-factor interaction between the device geometry and PNIPAM-AAm concentration.

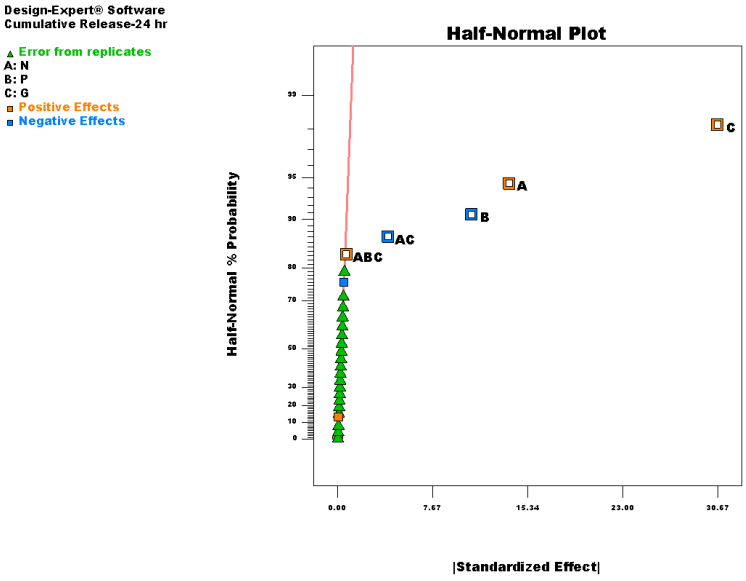

Figure 4.26 Half normal plot for cumulative protein release over 24 hours A (N) corresponds to the PNIPAM-AAM, B (P) corresponds to PEGDA and G corresponds to the device geometry (slit or cross).

Slit:

The equation for % cumulative protein released from the slit geometry during the 24 hours of thermal cycling in terms of actual factors and combined effect of factors is given below.

% Cumulative protein released over 24 hours = 91.66733 + (4.40383) N – (2.26347) P

+ (0.039033) NP

Where N is the PNIPAM-AAm concentration, P is the PEGDA concentration.

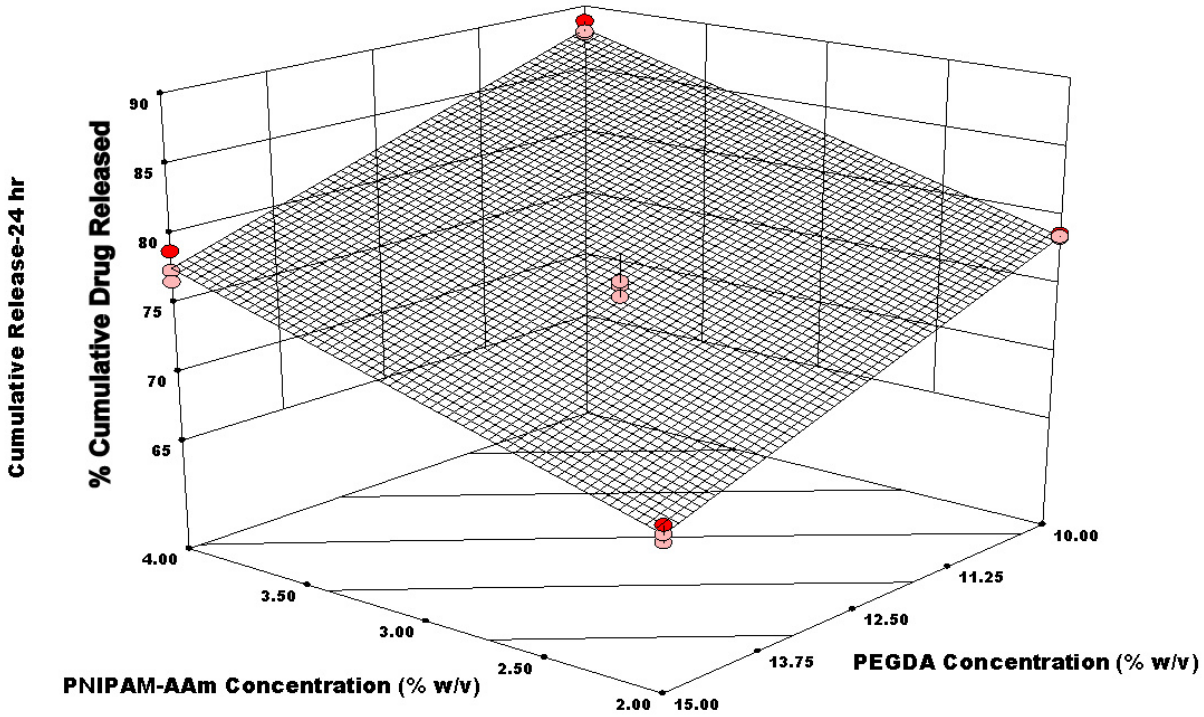

Figure 4.27 Response surface diagram for slit geometry for % cumulative release over 24 hour a function of PNIPAM-AAm and PEGDA concentration.

From Figure 4.27 the relation between the PNIPAM-AAm and PEGDA concentrations on the % cumulative protein released is seen. The negative effect of the PEGDA concentration counters the positive effect of the PNIPAM-AAm concentration. The response surface is planar, with the model reasonably well-fitted around the actual mid-point release percentages.

.

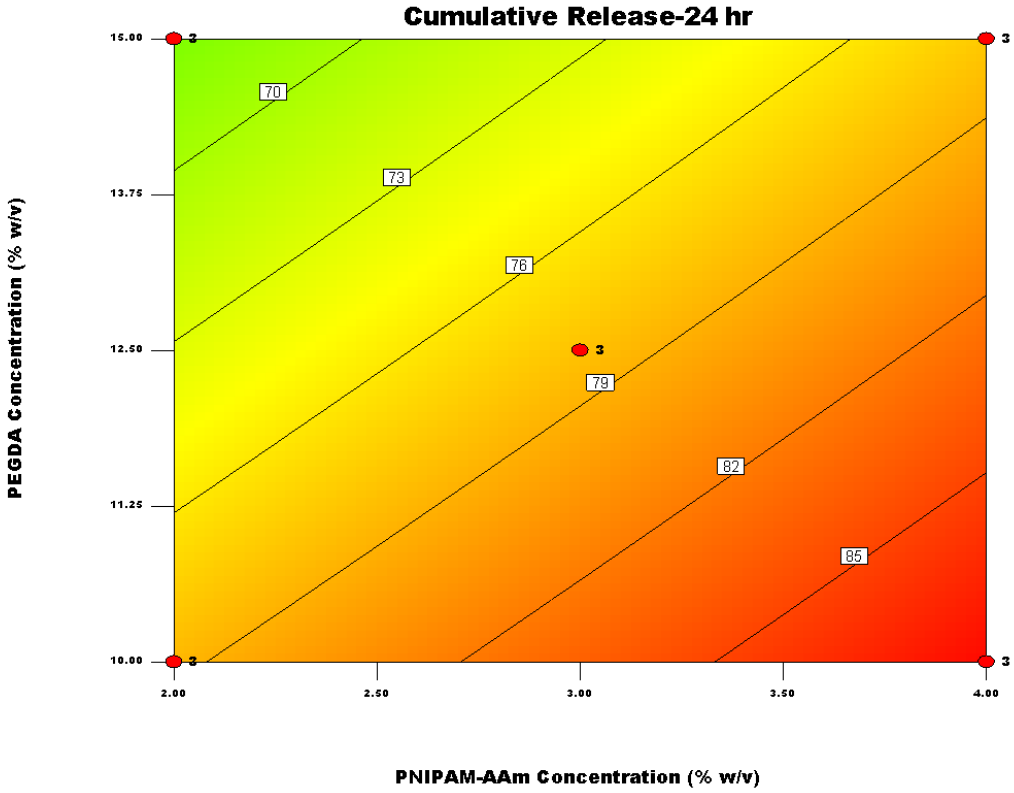

Figure 4.28 Contour plot for protein release rate from slit geometry for 24 hours of cumulative (%) release over 24 hours. The iso-contour lines are in %cumulative BSA released. The 45° angle of the iso-contour lines indicate equal effect of both the PNIPAM-AAm concentration as well as the PEGDA concentration.

A look at the contours for the cumulative release percentages confirms the linear variance of the response. The contours lines are at 45° indicating the effect of PEGDA and PNIPAM-AAm concentrations on the release rate of BSA.

Cross:

The equation for % cumulative protein released from the slit geometry during the 24 hours of thermal cycling in terms of actual factors and combined effect of factors is given below.

% Cumulative protein released over 24 hours = 91.66733 + (4.40383) N – (2.26347) P + (0.039033) NP

Where N is the PNIPAM-AAm concentration and P is the PEGDA concentration.

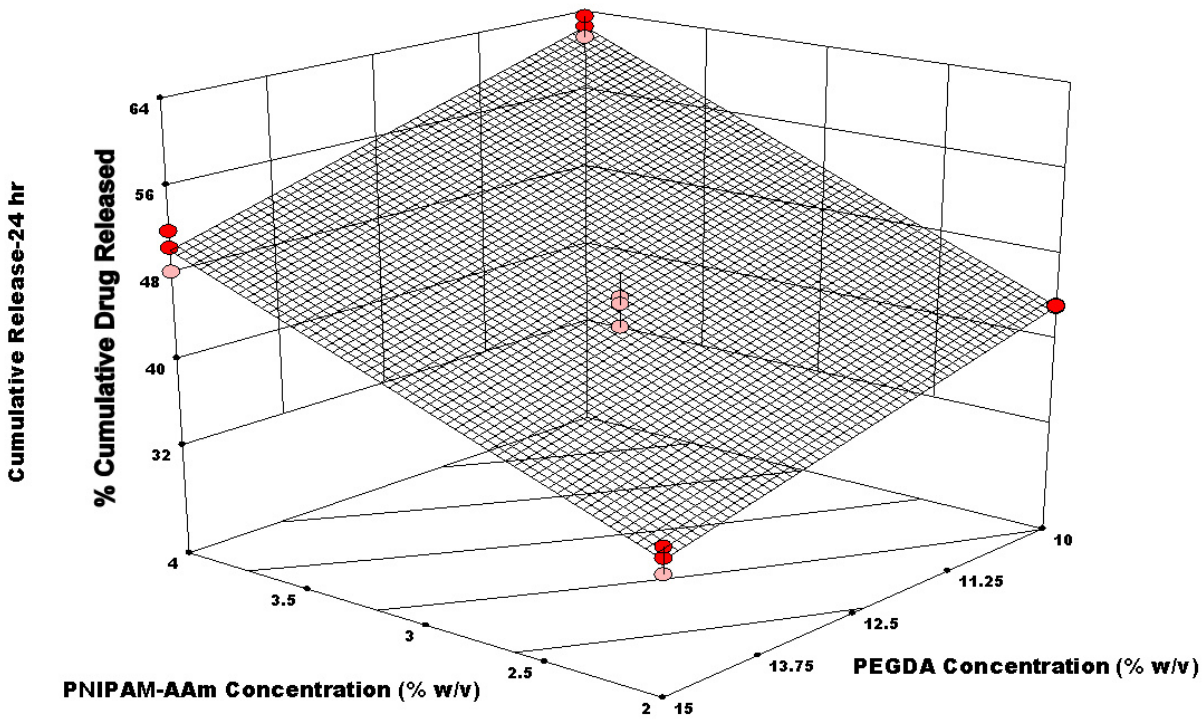

Figure 4.29 Response surface diagram for cross geometry for % cumulative release over 24 hours as a function of PNIPAM-AAm and PEGDA concentration.

For the cross geometry, the % cumulative protein released has a greater dependence on the PNIPAM-AAm nanoparticle concentration. Roughly 50% of the protein is released after 24 hours when the PNIPAM-AAm concentration is 4% (w/v) and PEGDA is at 15% (w/v) concentration. Only 44% is released when the concentrations are changed to 2% and 10% (w/v) of the PNIPAM-AAm and PEGDA, respectively. The response surface is planar, with the actual response for the midpoint concentrations lying slightly below the predicted surface curve.

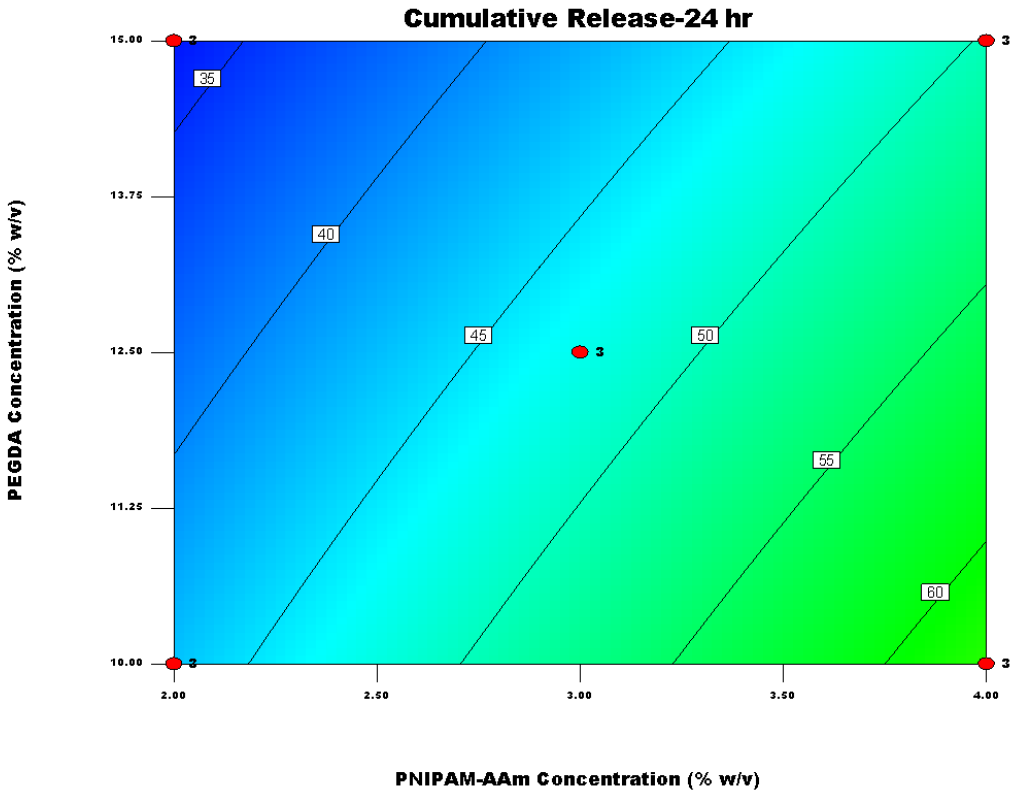

Figure 4.30 Contour plot for protein release rate from cross geometry for 24 hours of cumulative (%) release over 24 hours.

From Figure 4.30, it can be deduced that the response varies fairly linearly with the factors, but more sensitive to the PNIPAM-AAm concentration. To achieve a 50% cumulative release over 24 hours from the cross geometry, protein concentrations as low as 2.75% (w/v) can be used.

Discussion:

The cumulative protein release percentages over 24 hours of thermal cycling are higher for the slit geometry than the cross geometry. Thus, the geometry of the device plays a significant role in controlling the released amount of protein. While there is equal counter effect of the PNIPAM-AAm and PEGDA concentration on the response for the slit geometry, it is more dependent on the PNIPAM-AAm concentration for the cross geometry.

4.5 Discussion

In this study, a design of experiments approach utilizing a full factorial analysis was done on the effect of PNIPAM-AAm nanoparticle concentration, PEGDA concentration, and device geometry on the protein release rates and cumulative protein released from the thermoresponsive hydrogel-loaded devices developed and described in chapter 3, over a period of 24 hours of thermal cycling. A detailed study was done on the release rates during the initial stage of protein release (first two thermal cycles), as well as the release rates during steady state release.

In all the responses, the PNIPAM-AAm nanoparticle concentration was shown to have a positive effect on the response. A high PNIPAM-AAm nanoparticle concentration is directly related to the amount of BSA loaded in the hydrogel, thus a greater nanoparticle concentration leads to greater concentration gradients for the BSA during diffusion, and in general, a greater amount of BSA available to be released. Also, the PNIPAM-AAm nanoparticles directly control the degree of thermoresponsiveness of the system.

The PEGDA concentration was seen to have an inverse relationship with the protein release rates and amounts. It has been reported that a higher PEGDA concentration increases the cross-linking within the hydrogel system. [59]. Thus, increased cross-linking can lead to a denser, packed network, inhibiting the diffusion of the protein out from the hydrogel.

Individual factors were seen to play a more significant role, with some two-factor interactions having a minor effect on the response. 3-factor interactions were negligible.

With the exception of the 1st OFF cycle, the release rates from the slit geometry are higher in comparison the cross geometry. This behavior has already been explained in chapter 3. Geometries which have easier access to the edges as well as the center of the hydrogel release a larger amount of protein due to the thicker edges and slightly thinner height at the center of the hydrogel.

During the initial stages of protein release (1st and 2nd ON and OFF cycles), the slit geometry has an antagonistic effect between the PNIPAM-AAm and PEGDA concentration, the positive effect of the PNIPAM-AAm concentration countering the negative effect of the PEGDA concentration. However, the release rates from the cross geometry have a greater dependence on the PNIPAM-AAm nanoparticle

concentration, with linear dependence as well. This seems to be a geometry controlled release, since the device geometry is the primary factor altering the release rates for these cycles.

The release rates during the steady state ON cycle drop down from those observed in the 2nd ON cycle. During steady state, the hydrogels are in a phase of sustained release and past the burst release of the initial cycles. Here, the PNIPAM-AAm concentration enhances the release rate from the slit geometry, where as the PEGDA concentration limits the release rates from the cross geometry.

The % cumulative protein released over 24 hours of thermal cycling has linear variance with the PNIPAM-AAm and PEGDA concentrations for the slit geometry. Both the factors have an antagonistic effect on the cumulative protein released. For the cross geometry, cumulative protein released is more dependent on the PNIPAM-AAm concentration.

The response surface diagrams do not entirely fit around the experimental midpoint response values. Increasing the number of runs for different levels of the process parameters (PEGDA and PNIPAM-AAm concentration), might result in a better fit. Also, choosing a different model, e.g. D-optimal model instead of a full factorial analysis is also recommended for a better understanding of the complex relationships between the factors.

CHAPTER 5

SUMMARY AND FUTURE WORK

5.1 Summary

A temperature sensitive drug eluting device was developed in this study using a composite hydrogel of PNIPAM-AAm nanoparticles embedded in a PEGDA matrix. PNIPAM-AAm, which accounts for the thermo-sensitivity of the hydrogel, undergoes a reversible phase transition from a hydrophilic swollen state to a hydrophobic shrunken state expelling all water and protein/drugs loaded in it, when it is heated to its LCST. [12,13,19]. By adjusting the ratio of hydrophilic groups such as acryl amide (AAm), the LCST of the PNIPAM-AAm nanoparticles used in this study has been adjusted to 39-40° C.[26] . Studies show that this composite hydrogel is biocompatible [40]. The device was made using PMMA, with a base plate containing a cavity to hold the hydrogel and a cover plate with an orifice through which the release protein has to diffuse across into the release medium. The composite hydrogel properties have been used to control the release of drugs from this device, as can be seen in Figure 3.1 in Chapter 3. . Devices with four different device orifice geometries were fabricated – slit, cross, circle and four-circle. All geometries were centrally located over the hydrogel. BSA was used as the model protein for this research.

Continuous protein release from these devices as well as pulsatile release upon thermal cycling, above and below the LCST, was characterized. Continuous drug release studies from hydrogels made of PNIPAM and its copolymers have been well characterized in literature. [20, 55, 60, 61] However, in this study, the protein release characterized was that from the hydrogel loaded in the device. A pulsatile release over 24 hours was also characterized, to investigate the ON/OFF behavior desired of this device. Similar pulsatile release studies from hydrogels have been made. [9, 42, 47, 49, 62, 63] A comparative study was made between the protein release profiles for the different

device geometries. A significant contrast in the release profiles from the four geometries was observed. During continuous release, both above and below the LCST, the slit geometry device showed the highest cumulative protein release. The cross and the four-circle geometries released up to 10% of loaded BSA after 24 hours of continuous release at 23.1 °C, where as the release from the slit geometry (~35%) and circle geometry (~20%) was higher. It was postulated that the four-circle geometry had a lower release because the small dimensions of the orifice geometry greatly increased surface tension effects, making it harder for water to exit and enter through the opening. Above the LCST at 41 °C, the slit and four-circle geometries had a greater release in comparison to the other two geometries. This release behavior is observed because the slit and four-circle geometries provide easier access to the center as well as edges of the hydrogel, making it easier for the released protein to diffuse out.

During pulsatile release from the device, a step release curve was obtained, thus indicating that an ON/OFF release behavior was achievable. The release profile was divided into two stages of release, an initial release period comprising of the first two thermal cycles, and a steady state release stage, comprising of the remaining six thermal cycles. The initial release stage had higher protein release rates, due to a slight initial burst. During steady state release, the subsequent cycling above and below the LCST of the nanoparticles gives us more or less repetitive protein release amounts for each ON and OFF cycle. We do not observe a strictly OFF release below LCST, which can be explained by the reasoning that all the protein released in the ON phase may not diffuse out through the device, and instead some amount settles on the hydrogel surface when it swells again at room temperature.

A full factorial analysis using design of experiments to investigate the effects of PNIPAM-AAm concentration, PEGDA concentration and device geometry (slit and cross) on the release rates and cumulative protein release rate during pulsatile release over 24 hours was carried out. A synergistic-antagonistic effect of the PNIPAM-AAm concentration and PEGDA concentration on the release rate response and cumulative protein released response was observed. The PNIPAM-AAm enhanced the release rate whereas PEGDA limited it. A higher PEGDA concentration has been known to lead to

greater cross-linking [57]. Greater cross-links lead to a dense packed hydrogel, making it harder for loaded drugs to diffuse out through the hydrogel.

During the initial release stages (1st and 2nd OFF and ON cycles), the PNIPAM-AAm nanoparticle concentration had a greater effect on the protein release from the cross geometry. The release rates during the steady state ON cycle dropped down from those observed in the 2nd ON cycle. During steady state, the hydrogels are in a phase of sustained release and past the burst release of the initial cycles. Here, the PNIPAM-AAm concentration enhanced the release rate from the slit geometry, whereas the PEGDA concentration limited the release rates from the cross geometry. The % cumulative protein released over 24 hours of thermal cycling had a linear variance with the PNIPAM-AAm and PEGDA concentrations for the slit geometry. Both the factors were observed to have an antagonistic effect on the cumulative protein released. For the cross geometry, the cumulative protein released was more dependent on the PNIPAM-AAm concentration. Two-factor and three-factor interactions were found not to have a significant effect on the protein release rates. Equations for calculating the release rates for a desired set of input parameter conditions were also obtained from the full factorial model.

The drug delivery device developed is a promising step towards developing a temperature sensitive wound healing dressing for controlled drug delivery. The next section talks about suggested work based on this research and its findings.

5.2 Future Work

Following is a list of recommended work based on this research:

1. The center point response surfaces did not entirely confirm with the actual data points from the experimental runs in this experiment. This tells us that a much more complicated function would confirm better with the data points than the one generated by the full factorial model. Carrying out more number of runs for different mid value conditions is one way to improve the accuracy of the predicted behavior. Another alternative is to choose a different model altogether. Using a D-optimal

design is recommended since the pure D-optimal points are augmented in the design with additional runs that provide estimates of lack of fit and pure error.

2. An end-application wound healing dressing is required to be conformable around the body. A stiff material such as PMMA is not suitable for the purpose. Making a device out of conformable, biocompatible materials is essential to the device design. Poly (dimethyl siloxane) or PDMS has been used to fabricate wound dressings and patches and can be a material of choice. [8, 64]. Changing the material of device will change the release properties to an extent as well since surface properties will also change.
3. Creating a heating and cooling mechanism in the device itself to locally heat and cool specific rows of hydrogels. This way, different rows of hydrogels can be loaded with different therapeutic agents and their release can be modulated by controlling the local temperature.
4. Using actual therapeutic agents and monitoring their release from the device. The model drug used in this study was BSA. It was used since it has a molecular weight (66.7 kDa) similar to most physiological proteins. The diffusion kinetics will vary based on the therapeutic agents and their properties loaded in the hydrogel.
5. Conducting animal studies on the final developed device dressing to observe the physiological response to wound treatment via this method.

APPENDIX A

BSA STANDARD CURVE

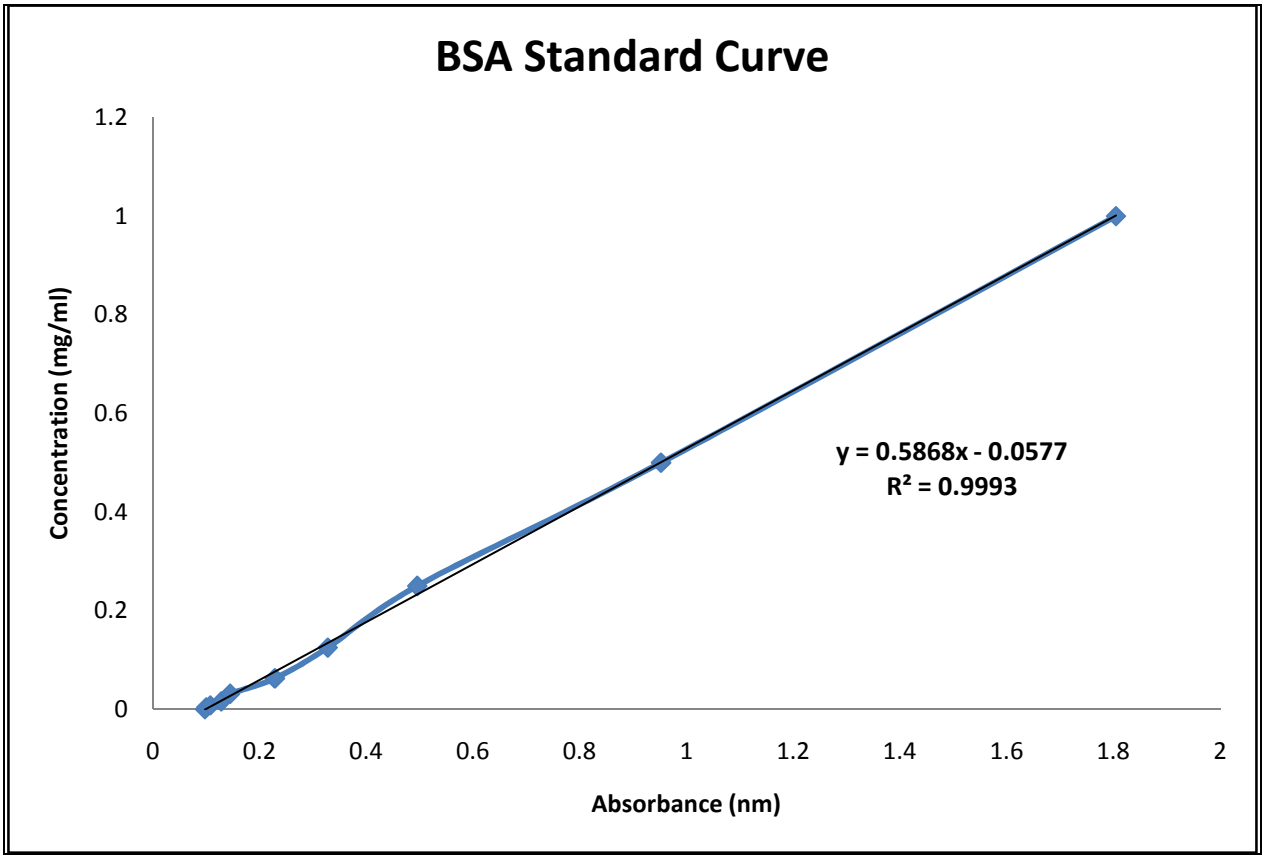
BSA Standard Curve
Concentration (mg/ml)
1.2
1
0.8
0.6
0.4
0.2
0
0
0.2
0.4
0.6
0.8
1
1.2
1.4
1.6
1.8
2
Absorbance (nm)
y = 0.5868x - 0.0577
R² = 0.9993

REFERENCES

[1] American Burn Association National Burn Repository (2010 report). Burn Incidence and Treatment in the United States: 2011 Fact Sheet
. 2010; 2011.

[2] Blakytny R, Jude E. The molecular biology of chronic wounds and delayed healing in diabetes. Diabetic Med 2006; 23:594-608.

[3] Winter GD. Formation of the Scab and the Rate of Epithelization of Superficial Wounds in the Skin of the Young Domestic Pig. Nature 1962; 193:293-294.

[4] Winter GD, Scales JT. Effect of Air Drying and Dressings on the Surface of a Wound. Nature 1963; 197:91-92.

[5] Hinman CD, Maibach H. Effect of Air Exposure and Occlusion on Experimental Human Skin Wounds. Nature 1963; 200:377-378.

[6] Bao P, Kodra A, Tomic-Canic M, Golinko MS, Ehrlich HP, Brem H. The Role of Vascular Endothelial Growth Factor in Wound Healing. J Surg Res 2009;153 :347-358.

[7] McGonigle JS, Tae G, Stayton PS, Hoffman AS, Scatena M. Heparin-regulated delivery of osteoprotegerin promotes vascularization of implanted hydrogels. Journal of Biomaterials Science, Polymer Edition 2008 ;19 :1021-1034.

[8] Jones V, Grey JE, Harding KG. Wound dressings. BMJ 2006 ;332 :777.

[9] Patel JD. Pulsatile Drug Delivery System: An "User-Friendly" Dosage Form. JPRHC April 2010 ;2 :204--215.

[10] Barrow RE, Herndon DN. History of treatments of burns. In: David N. Herndon, MD, FACS, editors. Total Burn Care (Third Edition)Edinburgh: W.B. Saunders, 2007. p. 1-8.

[11] Shakespeare P. Burn wound healing and skin substitutes. Burns 2001 ;27 :517-522.

[12] Peppas NA, Bures P, Leobandung W, Ichikawa H. Hydrogels in pharmaceutical formulations. European Journal of Pharmaceutics and Biopharmaceutics 2000 ;50 :27-46.

[13] Klouda L, Mikos AG. Thermoresponsive hydrogels in biomedical applications. European Journal of Pharmaceutics and Biopharmaceutics 2008 ;68 :34-45.

[14] Gupta P, Vermani K, Garg S. Hydrogels: from controlled release to pH-responsive drug delivery. Drug Discov Today 2002 ;7 :569-579.

[15] Murdan S. Electro-responsive drug delivery from hydrogels. J Controlled Release 2003 ;92 :1-17.

[16] Bajpai AK, Shukla SK, Bhanu S, Kankane S. Responsive polymers in controlled drug delivery. Progress in Polymer Science 2008 ;33 :1088-1118.

[17] Wu J, Liu S, Heng PW, Yang Y. Evaluating proteins release from, and their interactions with, thermosensitive poly (N-isopropylacrylamide) hydrogels. J Controlled Release 2005 ;102 :361-372.

[18] Inomata H, Saito S. Studies on volume phase transition of N-substituted acrylamide hydrogels. Fluid Phase Equilib 1993 ;82 :291-302.

[19] Ramanan RMK, Chellamuthu P, Tang L, Nguyen KT. Development of a Temperature-Sensitive Composite Hydrogel for Drug Delivery Applications. Biotechnol Prog 2006 ;22 :118-125.

[20] Sabnis A, Wadajkar AS, Aswath P, Nguyen KT. Factorial analyses of photopolymerizable thermoresponsive composite hydrogels for protein delivery. Nanomedicine: Nanotechnology, Biology and Medicine 2009 ;5 :305-315.

[21] Ramanan RMK, Chellamuthu P, Tang L, Nguyen KT. Development of a Temperature-Sensitive Composite Hydrogel for Drug Delivery Applications. Biotechnol Prog 2006 ;22 :118-125.

[22] Peppas NA, Keys KB, Torres-Lugo M, Lowman AM. Poly(ethylene glycol)-containing hydrogels in drug delivery. J Controlled Release 1999 ;62 :81-87.

[23] Cruise GM, Hegre OD, Scharp DS, Hubbell JA. A sensitivity study of the key parameters in the interfacial photopolymerization of poly(ethylene glycol) diacrylate upon porcine islets. Biotechnol Bioeng 1998 ;57 :655-665.

[24] Luna VH, Teymour F. Photopolymerization of Poly(Ethylene Glycol) Diacrylate on Eosin-Functionalized Surfaces. Langmuir 2004; 2004 ;20 :8652-8658.

[25] Peppas NA, Keys KB, Torres-Lugo M, Lowman AM. Poly(ethylene glycol)-containing hydrogels in drug delivery. J Controlled Release 1999 ;62 :81-87.

[26] Sousa RG, Magalhães WF, Freitas RFS. Glass transition and thermal stability of poly(N-isopropylacrylamide) gels and some of their copolymers with acrylamide. Polym Degrad Stab 1998 ;61 :275-281.

[27] Ather S, Chan DS, Harding KG. The biology of wound healing. EJHPPractice 2007 ;13 :53.

[28] Greenhalgh DG. The role of apoptosis in wound healing. Int J Biochem Cell Biol 1998 ;30 :1019-1030.

[29] Rovee DT. Evolution of wound dressings and their effects on the healing process. Clin Mater 1991 ;8 :183-188.

[30] Green H, Kehinde O, Thomas J. Growth of cultured human epidermal cells into multiple epithelia suitable for grafting. Proceedings of the National Academy of Sciences; Proceedings of the National Academy of Sciences 1979 ;76 :5665-5668.

[31] Berger J, Reist M, Mayer JM, Felt O, Peppas NA, Gurny R. Structure and interactions in covalently and ionically crosslinked chitosan hydrogels for biomedical applications. European Journal of Pharmaceutics and Biopharmaceutics 2004 ;57 :19-34.

[32] Park H, Park K. Biocompatibility Issues of Implantable Drug Delivery Systems. Pharm Res 01;13 :1770-1776-1776.

[33] Hoare TR, Kohane DS. Hydrogels in drug delivery: Progress and challenges. Polymer 2008 ;49 :1993-2007.

[34] Fix JA. Oral Controlled Release Technology for Peptides: Status and Future Prospects. Pharm Res 01;13 :1760-1764-1764.

[35] Peppas NA. Hydrogels and drug delivery. Current Opinion in Colloid & Interface Science 1997 ;2 :531-537.

[36] Bartil T, Bounekhel M, Cedric C, Jeerome R. Swelling behavior and release properties of pH-sensitive hydrogels based on methacrylic derivatives. Acta Pharmaceutica 2007 ;57 :301-314.

[37] Jeong B, Gutowska A. Lessons from nature: stimuli-responsive polymers and their biomedical applications. Trends Biotechnol 2002 ;20 :305-311.

[38] Satarkar NS, Hilt JZ. Magnetic hydrogel nanocomposites for remote controlled pulsatile drug release. J Controlled Release 2008 ;130 :246-251.

[39] Ramanathan S, Block LH. The use of chitosan gels as matrices for electrically-modulated drug delivery. J Controlled Release 2001 ;70 :109-123.

[40] Na K, Park JH, Kim SW, Sun BK, Woo DG, Chung H, et al. Delivery of dexamethasone, ascorbate, and growth factor (TGF [beta]-3) in thermo-reversible hydrogel constructs embedded with rabbit chondrocytes. Biomaterials 2006 ;27 :5951-5957.

[41] Tokuyama H, Kato Y. Preparation of thermosensitive polymeric organogels and their drug release behaviors. European Polymer Journal 2010 ;46 :277-282.

[42] Kikuchi A, Okano T. Pulsatile drug release control using hydrogels. Adv Drug Deliv Rev 2002 ;54 :53-77.

[43] Cappello J, Crissman JW, Crissman M, Ferrari FA, Textor G, Wallis O, et al. In-situ self-assembling protein polymer gel systems for administration, delivery, and release of drugs. J Controlled Release 1998 ;53 :105-117.

[44] Mittur A. Temperature modulation of transdermal drug delivery. , 2006.

[45] Varghese JM, Ismail YA, Lee CK, Shin KM, Shin MK, Kim SI, et al. Thermoresponsive hydrogels based on poly(N-isopropylacrylamide)/chondroitin sulfate. Sensors Actuators B: Chem 2008 ;135 :336-341.

[46] Zhang J, Chu L, Li Y, Lee YM. Dual thermo- and pH-sensitive poly(N-isopropylacrylamide-co-acrylic acid) hydrogels with rapid response behaviors. Polymer 2007 ;48 :1718-1728.

[47] Coughlan DC, Quilty FP, Corrigan OI. Effect of drug physicochemical properties on swelling/deswelling kinetics and pulsatile drug release from thermoresponsive poly(N-isopropylacrylamide) hydrogels. J Controlled Release 2004 ;98 :97-114.

[48] Cleland JL, Daugherty A, Mrsny R. Emerging protein delivery methods. Curr Opin Biotechnol 2001 ;12 :212-219.

[49] Brazel CS, Peppas NA. Pulsatile local delivery of thrombolytic and antithrombotic agents using poly(N-isopropylacrylamide-co-methacrylic acid) hydrogels. J Controlled Release 1996 ;39 :57-64.

[50] Lue SJ, Hsu J, Chen C, Chen B. Thermally on–off switching membranes of poly(N-isopropylacrylamide) immobilized in track-etched polycarbonate films. J Membr Sci 2007 ;301 :142-150.

[51] Dinarvand R, D'Emanuele A. The use of thermoresponsive hydrogels for on-off release of molecules. J Controlled Release 1995 ;36 :221-227.

[52] Li SK, D'Emanuele A. Effect of thermal cycling on the properties of thermoresponsive poly(N-isopropylacrylamide) hydrogels. Int J Pharm 2003 ;267 :27-34.

[53] Peppas NA, Keys KB, Torres-Lugo M, Lowman AM. Poly(ethylene glycol)-containing hydrogels in drug delivery. J Controlled Release 1999 ;62 :81-87.

[54] Kim SW, Bae YH, Okano T. Hydrogels: Swelling, Drug Loading, and Release. Pharm Res 01;9 :283-290-290.

[55] Cuggino JC, Strumia MC, Alvarez Igarzabal CI. Synthesis, characterization and slow drug delivery of hydrogels based in N-acryloyl-tris-(hydroxymethyl) aminomethane and N-isopropyl acrylamide. React Funct Polym 2011 ;71 :440-446.

[56] Yoshida R, Kaneko Y, Sakai K, Okano T, Sakurai Y, Bae YH, et al. Positive thermosensitive pulsatile drug release using negative thermosensitive hydrogels. Journal of Controlled Release 1994 ;32 :97--102.

[57] Ghosh K, Shu XZ, Mou R, Lombardi J, Prestwich GD, Rafailovich MH, et al. Rheological Characterization of in Situ Cross-Linkable Hyaluronan Hydrogels. Biomacromolecules 2005; 2005 ;6 :2857-2865.

[58] Fisher RA. The design of experiments. Oliver and Boyd, Edinburgh; London, 1935.

[59] Ghosh K, Shu XZ, Mou R, Lombardi J, Prestwich GD, Rafailovich MH, et al. Rheological Characterization of in Situ Cross-Linkable Hyaluronan Hydrogels. Biomacromolecules 2005; 2005 ;6 :2857-2865.

[60] Wei H, Cheng S, Zhang X, Zhuo R. Thermo-sensitive polymeric micelles based on poly(N-isopropylacrylamide) as drug carriers. Progress in Polymer Science 2009 ;34 :893-910.

[61] Guo B, Gao Q. Preparation and properties of a pH/temperature-responsive carboxymethyl chitosan/poly(N-isopropylacrylamide)semi-IPN hydrogel for oral delivery of drugs. Carbohydr Res 2007 ;342 :2416-2422.

[62] LoPresti C, Vetri V, Ricca M, Foderà V, Tripodo G, Spadaro G, et al. Pulsatile protein release and protection using radiation-crosslinked polypeptide hydrogel delivery devices. React Funct Polym 2011 ;71 :155-167.

[63] Li SK, D'Emanuele A. Effect of thermal cycling on the properties of thermoresponsive poly(N-isopropylacrylamide) hydrogels. Int J Pharm 2003 ;267 :27-34.

[64] Intra J, Glasgow JM, Mai HQ, Salem AK. Pulsatile release of biomolecules from polydimethylsiloxane (PDMS) chips with hydrolytically degradable seals. J Controlled Release 2008 ;127 :280-287.

BIOGRAPHICAL INFORMATION

The author, Shruti Gandhi, was born in the small town of Nagda, India, but has had the good fortune of being raised in a number of cities around the world. Coming from a family of engineers, “tech-jargon” was regular dinner table conversation during her growing up years and it came as no surprise when, due to her aptitude for scientific studies, she joined the Bachelors in Technology program in Chemical Engineering at one of India’s leading technological institutes, National Institute of Technology, Surat in 2004. During her undergraduate studies, she became inclined towards the field of polymers, bioengineering and environmental science, which persuaded her to work on projects concerning nano-porous materials, nanoparticles for drug delivery, petrochemicals and biotechnology. In order to further pursue her interests, she joined the graduate program in Materials Science and Engineering at the University of Texas at Arlington in 2008 and started focusing her work on biomaterials and polymers. Awarded as a university scholar, she is a member of the Golden Key Honor Society. She is currently working on 2-3 papers in the field of drug delivery from hydrogels and wishes to continue doing challenging work and make a significant contribution to the field of science.